International Journal of Nanomedicine

Dovepress
open access to scientific and medical research

Open Access Full Text Article

ORIGINAL RESEARCH

ApoSEVs-Mediated Modulation of Versatile Target Cells Promotes Diabetic Wound Healing: Unveiling a Promising Strategy

Jian Yang[1,*], Xuanhao Zhang[1,2,*], Guanyu Wang[1,2], Shixing Ma[1,2], Yejia Yu[1], Chengcheng Liao[1], Zhuo Wang[1,2], Cheng Liang[1], Maojiao Li[1,2], Weidong Tian[1,2], Li Liao[1,2]

[1]State Key Laboratory of Oral Diseases & National Clinical Research Center for Oral Diseases & Engineering Research Center of Oral Translational Medicine, Ministry of Education & National Engineering Laboratory for Oral Regenerative Medicine, West China Hospital of Stomatology, Sichuan University, Chengdu, 610041, People's Republic of China; [2]Department of Oral and Maxillofacial Surgery, West China Hospital of Stomatology, Sichuan University, Chengdu, 610041, People's Republic of China

*These authors contributed equally to this work

Correspondence: Li Liao; Weidong Tian, State Key Laboratory of Oral Disease, West China School of Stomatology, Sichuan University, No. 14, 3Rd Section of Ren Min Nan Road, Chengdu, Sichuan, 610041, People's Republic of China, Tel +86-28-85503499; +86-28-85501256, Email lliao@scu.edu.cn; drtwd@sina.com

Background: Diabetic chronic wounds present a formidable challenge in clinical management, lacking effective treatment options. Mesenchymal stem cell (MSC) transplantation has emerged as a promising therapy for tissue repair and regeneration. However, transplanted MSCs often undergo rapid apoptosis, giving rise to heterogeneous extracellular vesicles (EVs), including apoptotic bodies (apoBDs) and apoptotic small extracellular vesicles (apoSEVs). The potential stimulatory role of these EVs in diabetic wound healing remains unknown.

Methods: In this study, we investigated the effects of apoSEVs derived from adipose-derived mesenchymal/stromal cells (ADSCs) on the recovery of diabetic wounds by modulating the function of versatile target cells. First, we characterized the apoSEVs and apoBDs derived from apoptotic ADSCs. Subsequently, we evaluated the effects of apoSEVs and apoBDs on macrophages, endothelial cells, and fibroblasts, three essential cell types in wound healing, under high-glucose conditions. Furthermore, we developed a gelatin methacryloyl (GelMA) hydrogel for the sustained release of apoSEVs and investigated its therapeutic effects on wound healing in type 2 diabetic mice in vivo.

Results: apoSEVs facilitated the polarization of M1 phenotype macrophages to M2 phenotype, promoted proliferation, migration, and tube formation of endothelial cells, and enhanced fibroblast proliferation and migration. However, apoBDs failed to improve the function of endothelial cells and fibroblasts. In vivo, the apoSEVs-loaded GelMA effectively promoted wound healing by facilitating collagen fiber deposition, angiogenesis, and immune regulation.

Conclusion: Our study elucidates the beneficial effects of apoSEVs on wound recovery in diabetes and introduces a novel strategy for diabetic wound treatment based on apoSEVs.

Keywords: apoptotic small extracellular vesicles, wound healing, diabetes, stem cells, GelMA

Introduction

Diabetic chronic wounds are among the most challenging complications of Diabetes mellitus (DM).[1–3] These wounds pose significant problems due to their prolonged treatment duration, high cost, and resulting disability, leading to substantial physical, psychological, and economic burdens.[4,5] Furthermore, diabetic chronic wounds frequently exhibit infection or deep tissue damage, making them the leading cause of non-traumatic amputations.[6] The overall mortality rate within 5 years for Diabetic foot ulcers (DFUs) is nearly 50%, and approximately 20% of moderate to severe DFUs eventually require amputation.[7] Despite the proposal of various innovative wound repair methods, such as local negative

Received: 14 September 2023
Accepted: 9 November 2023
Published: 22 November 2023

Graphical Abstract

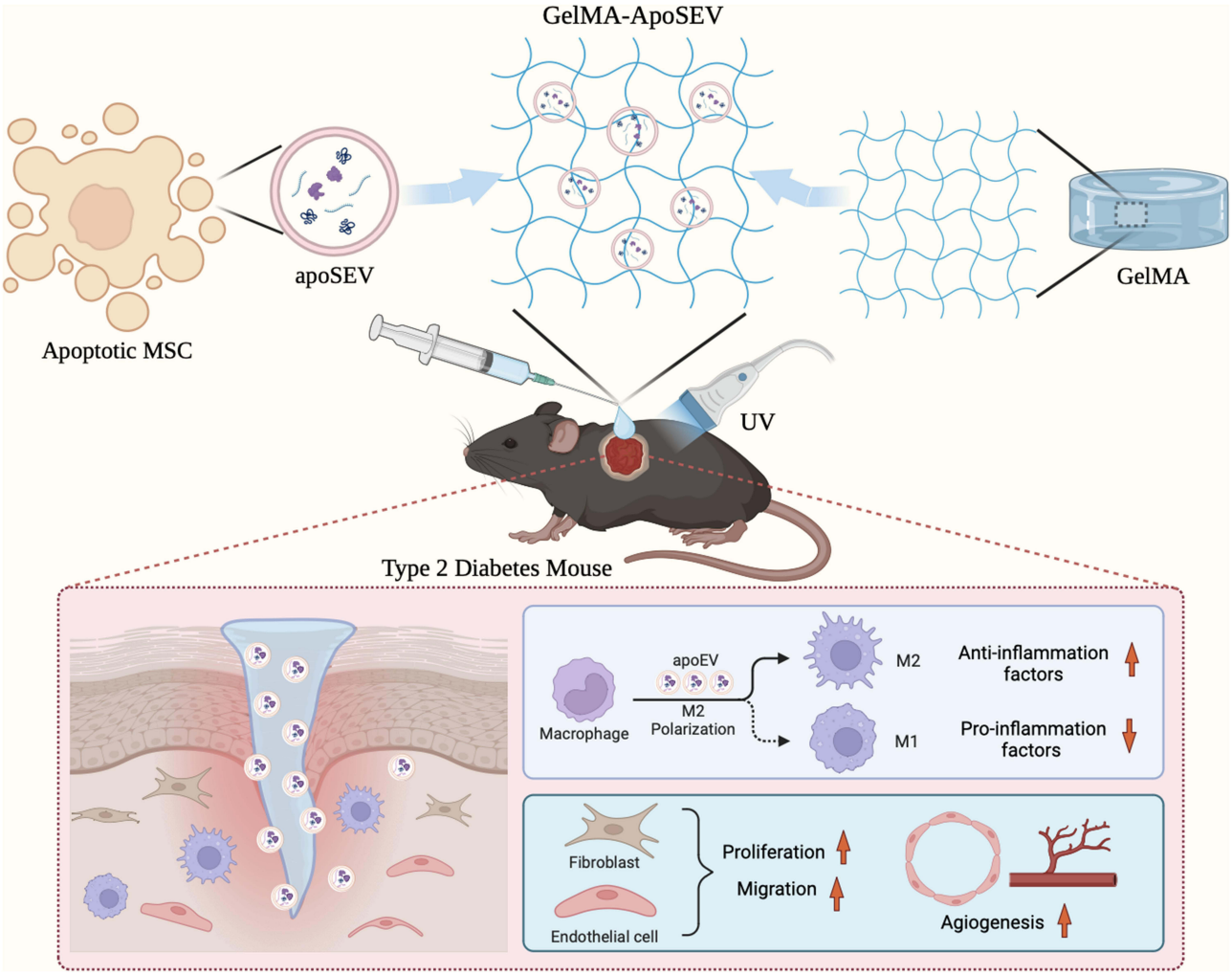

pressure, growth factors, and autologous platelet-rich gel, these conventional treatments often prove ineffective for many patients due to impaired cell function around the wound site resulting from underlying microenvironmental alterations.[8,9]

The wound healing process relies on a dynamic chain of physiological events, including hemostasis, inflammation, proliferation, and remodeling. Any disruption in this process, such as excessive inflammation and dysfunction of cells involved in repair due to a high glucose environment, leads to delayed wound healing and the development of chronic wounds.[10,11] Impaired wound healing in diabetes stems from the dysfunction of cells associated with the wound, induced by hyperglycemia.[2] Inflammatory cell dysfunction and dysregulated inflammatory factors characterize the inflammation phase of diabetic wound healing. The hyperglycemic microenvironment leads to macrophage dysfunction and persistent polarization towards the pro-inflammatory M1 phenotype, while inflammatory factors become dysregulated, resulting in a sustained inflammatory state that hampers wound healing.[12] The proliferative phase of diabetic wound healing is marked by impaired physiological function of fibroblasts and endothelial cells, leading to compromised granulation tissue formation and angiogenesis, which further impede wound healing.[13] Consequently, addressing persistent inflammation, impaired cell proliferation and migration, and diminished angiogenesis is crucial for the management of refractory or contraindicated wounds. This necessitates the exploration of more targeted treatment options.

Cytotherapy of mesenchymal stem cells (MSCs) have emerged as a promising therapy and have shown favorable effects on accelerating the healing of diabetic skin wounds and restoring skin integrity.[14,15] Traditionally, it was believed that MSCs function through self-renewal and paracrine regulation after homing.[16–20] However, recent studies have reported extensive apoptosis of transplanted MSCs shortly after transplantation. These dead MSCs were uptaken by local cells through a process of efferocytosis, which eventually clear the apoptotic MSCs. Emerging evidence showed efferocytosis of the apoptotic MSCs would perform profound effect on the recipient cells, including macrophage, fibroblast, and others.[21–23]

During the process of apoptosis, a significant quantity of heterogenous apoptotic extracellular vesicles (apoEVs) is generated.[24–26] These apoEVs include large vesicles named apoptotic bodies (apoBDs), vesicles ranging from 1 to 5 μm in size,[27,28] and smaller membrane-bound vesicles, namely apoptotic microvesicles (apoMVs) with a diameter of 0.1−1 μm and apoptotic exosomes (apoExos) with a diameter of less than 150 nm. These smaller vesicles are collectively referred to as apoptotic small extracellular vesicles (apoSEVs).[28,29]

Previous studies predominantly focused on ApoBDs have demonstrated ApoBDs restore tissue homeostasis and promote tissue repair by facilitating angiogenesis and immune regulation.[30,31] A previous study has confirmed the regulatory role of apoBDs in wound healing.[21] The latest study has shown that apoBDs could be efferocytosed by macrophages and functionally modulate liver macrophage homeostasis to counteract T2D.[32] But due to their large size, apoBDs is mainly engulfing by macrophage.

With a significantly smaller size, apoSEVs can be efferocytosed by various types of cells, including macrophages, fibroblasts, mesenchymal stem cells, endothelial cells, and others.[31,33] Furthermore, apoSEVs carry a wealth of proteins, RNA, DNA, lipids, and more, and can perform essential functions once taken up by recipient cells.[34] However, the precise role of apoSEVs in wound healing requires further exploration and elucidation.

In this study, we extensively investigated the biological of apoSEVs of adipose-derived stem cells (ADSCs) in wound healing. Our results confirm that apoSEVs derived from ADSCs exert positive effects on essential cells involved in the inflammatory and proliferative phases, namely macrophages, endothelial cells, and fibroblasts, in vitro. Subsequently, we applied a novel dressing composed of apoSEVs and GelMA hydrogel to an in vivo model of diabetic skin wounds, which exhibited remarkable healing effects. ApoSEVs treatment holds promise as a potential therapeutic approach to expedite the healing of diabetes-related skin wounds.

Materials and Methods

Cell Culture

The cell lines of Raw264.7 and HUVECs were purchased from the Cell Bank of the Chinese Academy of Sciences. Raw264.7 and HUVECs were cultured in high glucose DMEM (Gibco) supplemented with 10% Fetal Bovine Serum (FBS, Gibco, USA) and 100 U/mL penicillin, and 100 g/mL streptomycin. All the cells were cultured in condition at 37°C, 5% CO_2.

ADSCs were isolated according to the previous literature.[35] All procedures were reviewed and approved by the Ethics Committees of the State Key Laboratory of Oral Diseases, West China School of Stomatology, Sichuan University (approval number: WCHSIRB-D-2021-028). The informed consent was obtained from the study participants and the guidelines outlined in the Declaration of Helsinki were followed. Briefly, 100mL of adipose tissue from abdominal liposuction was washed with PBS, adding 2% of penicillin and streptomycin. Then, the tissue would be digested with collagenase type I (1 mg/mL) for 30 min, at 37 °C shaker. The cell suspension was centrifuged at 1200 rpm for 5 min accompanied by the same volume of α-MEM. Cell precipitation was resuspended in α-MEM (supplemented with 10% of FBS, 1% of penicillin and streptomycin) and added in 75 cm^2 culture flasks. Cells were cultured at 37 °C, 5% CO_2. The culture medium was then replaced every two days. When ADSCs were cultivated at 90% confluence, cells were detached with trypsin and seeded as Passage-1 cells. ADSCs before Passage-5 were used only.

Isolation and Characterization of apoSEV, EV, and apoBD

To isolate apoSEV and apoBD, ADSCs were exposed to 300 nM staurosporine (STS, Enzo Life Sciences) in serum-free medium for 12 hours to induce apoptosis. Apoptosis was confirmed through changes in cell morphology,

analysis of flow cytometry, and staining analysis of terminal deoxynucleotidyl transferase dUTP nick end labeling (TUNEL, Beyotime Biotechnology, China). Subsequently, the supernatant from apoptotic cells underwent centrifugation at 800 x g for 10 minutes to eliminate cell debris and at 3000 x g for 20 minutes to collect apoBD pellets. The remaining supernatant was then centrifuged at 16,000 x g for 30 minutes to isolate apoSEV in the pellet. For the isolation of EVs, a method based on our previous literature was utilized.[36] Briefly, ADSCs were cultured in medium without serum for 24 hours. The culture medium was first collected, followed by centrifugation at 2000 x g for 10 minutes to remove cellular debris. The resulting supernatants were then subjected to centrifugation at 10,000 x g for 30 minutes and subsequently at 100,000 x g for 70 minutes to obtain EV pellets. These pellets were then washed twice with PBS.

Transmission electron microscopy (TEM) was employed to examine the morphology of apoSEV and apoBD. Approximately 2 μL of each sample droplet was placed and adsorbed onto Formvar-carbon electron microscopy grids, followed by a 10-minute incubation at room temperature to facilitate nonspecific particle binding. Subsequently, the grids were washed with MilliQ water and then immersed in a uranyl acetate solution with a pH of 7 for approximately 3 min. After removing excess fluid using filter paper, the grids were air-dried. Imaging was performed using a Jeol 1010 electron microscope (JEM-1400PLUS, USA).

The particle concentration and size distribution of apoSEV were determined using Nanoparticle Tracking Analysis (NTA, Particle Metrix, Germany). The experiment was conducted following the manufacturer's manual. Samples were diluted in ultrapure water at ratios ranging from 1:100 to 1:10,000. All samples were measured in duplicate with consistent instrument settings. Measurements were carried out in 488 nm laser scatter mode, and the data were analyzed using ZetaView software 8.02.31.

For apoptotic marker detection, apoSEVs and apoBDs were characterized by Western blotting using the antibody Caspase-3 (#9664, Cell Signaling Technology). The BCA Protein Assay Kit (TIANGEN, China) was used to quantify the protein concentration of ApoSEV, EV, and apoBD.

For in vitro experiments, apoSEV, EV, and apoBD were introduced into fresh culture medium at 20 μg/mL. For in vivo experiments, 50 μg apoSEV and EV were mixed in 150 μL GelMA solution.

Macrophage Polarization and Immunofluorescence Detection

RAW264.7 cell line were cultured in DMEM with high glucose and supplementing with 10% FBS and 1% penicillin and streptomycin. Five groups were divided: the PBS group, LPS group (lipopolysaccharide, Sigma Aldrich, at 100 ng/mL, for 24 h), LPS + apoSEV group (apoSEVs at 20 μg/mL), LPS+EV (EVs at 20 μg/mL), LPS+apoBD (apoBD at 20 μg/mL). Cells were initially seeded into confocal dishes and then incubated at 37°C with 5% CO2. After 24 hours, the cells were washed with PBS and fixed with 4% PFA for 30 minutes at room temperature. Following another PBS wash, blocking was performed using goat serum for 30 minutes at room temperature. Subsequently, the cells were incubated overnight at 4°C with the following primary antibodies and corresponding secondary antibodies: anti-F4/80 (Santa Cruz, sc-25830) conjugated with Alexa Fluor 647 (Life tech, A31573), anti-CD206 (Santa Cruz, sc-58986) conjugated with Alexa Fluor 488 (Life tech, A11001), and anti-NOS2 (Santa Cruz, sc-7271) conjugated with Alexa Fluor 555 (Life tech, A21422). After another round of PBS washing, the cells underwent nuclei counterstaining with DAPI (Sigma-Aldrich, USA) for 10 min at room temperature. Finally, following further PBS washing, the cells were preserved using an anti-fade mounting medium. Fluorescence imaging was performed with a confocal laser scanning microscope from Olympus, and the analysis was conducted using ImageJ software.

The Isolation of Total RNA and qRT-PCR Analysis

To quantify the relative gene expressions of iNOS, IL-1β, TNF-α, IL-6, TGFβ, CD206 and IL-10, quantitative real-time polymerase chain reaction (qRT-PCR) were employed. In brief, total RNA was extracted from RAW264.7 cells using TRIzol reagent (Invitrogen). Subsequently, complementary DNA (cDNA) was synthesized through reverse transcription of the extracted total RNA using the Prime Script RT reagent Kit (Vazyme Biotech). For qRT-PCR analysis, we utilized the SYBR Green detection reagent (Vazyme Biotech). Finally, the 2-(ΔΔCT) method were used to determine the relative expression levels.

Cell Proliferation Assay

The cell proliferation was assessed by cell counting kit-8 (CCK-8) assay (KeyGen Bio TECH) according to the manufacturer's protocol. 2×10^3 per well cells were seeded into 96-well plates and treated with PBS, apoSEV (20 μg/mL), EV (20 μg/mL), and apoBD (20 μg/mL), respectively, for 7 days constantly. The automated plate reader were used to detect the optical density (OD) values at 450 nm.

Cell Migration Assay

For the scratch assay, Human Umbilical Vein Endothelial Cells (HUVECs) and Human Dermal Fibroblasts (HDFs) were seeded at a density of 5×10^5 cells per well into 6-well plates. Once the cells reached 90% confluence, using sterile 200 μL pipette tips to create scratches on the plates by gently scraping away the cells. Subsequently, the plates were washed with PBS, and the culture medium was replaced with a medium containing different vesicles, all at a concentration of 20 μg/mL. Scratch images were captured at 0, 12, and 24 hours using an inverted microscope. The quantification of the scratch area was conducted using ImageJ software.

For the transwell assay, HUVECs and HDFs were prepared in serum-free medium at a concentration of 5×10^3 cells/mL. Next, 100 μL of this cell suspension was added to the upper chamber of 24-well plates, which were equipped with an 8.0 μm polycarbonate membrane. In the lower chamber, medium containing various vesicles, similar to those used in the cell scratch assay, was added. After a 24-hour incubation period at 37°C with 5% CO2, the cells from the upper chamber's microporous membrane were carefully removed, and the migrated cells were stained with 0.1% crystal violet for 5 minutes. Subsequently, an optical microscope was utilized to observe and capture images of the stained cells.

Tube Formation Assay

To assess the formation of capillary networks, we conducted an in vitro tube formation assay using ibidi angiogenesis μ-Slides (ibidi, Germany) pre-coated with Matrigel (Corning, USA). 2×10^5 cells/mL HUVECs were seeded with 50 μL of medium in each well and incubated in culture FBS-free medium. The different treatments with vesicles were consistent with those described in the migration assay. Tube formation was captured through microscopy at the 4-hour mark using an inverted microscope. The quantification of network structures was performed by measuring five randomly selected microscopic fields using ImageJ software.

Preparation of GelMA/GelMA+apoSEV Hydrogels

GelMA and LAP photoinitiators were procured from Suzhou Engineering Life Co., LTD., China. A LAP photoinitiators standard solution was created using PBS at a 0.25% working concentration, which was subsequently employed to prepare GelMA solutions at varying concentrations. The prepared GelMA solution underwent sterilization via filtration through a 0.22 μm filter. To form composite GelMA+apoSEV hydrogels, ApoSEV pellets were blended with the GelMA solution and chemically cross-linked using ultraviolet radiation.

Analysis of Swelling Ratio and Storage and Loss Modulus

Cross-linked samples, measuring 10 mm in diameter and 5 mm in height, were submerged in PBS and left to incubate at 37°C for 24 h. After removing excess surface water, the swollen samples were weighed at designated time intervals. To determine the swelling ratios of the hydrogels, we applied the following formula: swelling ratio = [(weight of swollen hydrogels - initial dry weight) / initial dry weight] × 100%. The storage and loss modulus were accessed by the dynamic shear rheometer.

Degradation Behavior Assay

Cylindrical cross-linked samples, measuring 10 mm in diameter and 5 mm in height, were immersed in PBS containing 20U of collagenase at 37°C. These samples were collected at specified time intervals and subsequently rinsed with distilled water. Afterward, the samples underwent freeze-drying, and the excess mass was weighed. To determine the

degradation ratios of the hydrogels, we utilized the following formula: degradation ratio = (surplus weight of the hydrogels / initial weight) × 100%.

Cytotoxicity Assays for GelMA

Different concentrations of cross-linked GelMA samples were introduced into the upper chambers of 24-well plates, featuring an 8.0 μm polycarbonate membrane. In the lower chambers, ADSC cells were seeded at a density of 2×10^4 cells per well. To evaluate cytotoxicity, we employed the cell counting kit-8 (CCK-8) assay. Specifically, 20 μL of CCK-8 solution was added to 200 μL of culture medium in each well and incubated for an additional hour. The optical density (OD) values were then measured at 450 nm using an automated plate reader. This assay was conducted continuously over a span of 7 days.

Establishment of Skin Defect Model in Diabetic Mice and Treatment with GelMA +apoSEV

We obtained BKS-Dock Leprem2Cd479, DB/db male mice aged 8 weeks from GemPharmatech Co., Ltd. (Chengdu, China) and maintained them under standard experimental animal housing conditions. All experimental protocols and procedures were granted approval by the Ethics Committees of the State Key Laboratory of Oral Diseases, West China School of Stomatology, Sichuan University (Approval No. WCHSIRB-D-2023-036), and in accordance with the Guidelines for the Ethical Review of Laboratory Animal Welfare (GB/T 35892–2018). The mice were anesthetized using 4% chloral hydrate, and full-thickness skin wounds with a diameter of 10 mm were surgically created on their backs. The mice were divided into four groups randomly: (1) Control, (2) GelMA, (3) GelMA+EV, and (4) GelMA +apoSEV to assay the therapeutic effects of GelMA+apoSEV. In Control group, mice were treated with PBS at wound site. In GelMA group, mice were treated with 150 μL GelMA in wound site. In the GelMA+EV and GelMA+apoSEV, mice were treated with 150 μL GelMA containing 50 μg of EV or apoSEV protein content, respectively. On the day of surgery, GelMA solution was applied to the wounds and subsequently cross-linked using ultraviolet radiation for a duration of 10 seconds. Wounds in each experimental group were photographed on days 0, 4, 7, 10, and 14. The wound areas were quantified using Image software with the assistance of a ruler for reference. After 14 days, the mice were humanely euthanized under anesthesia induced by 10% chloral hydrate, and the healing wound tissues were collected for further analysis.

Histological Analysis

Tissues were fixed, dehydrated, and embedded in paraffin by histochemical methods. The embedded tissues were cut into 7 μm thick sections and stained with hematoxylin and eosin (H&E) kit (Solarbio, China) and Masson's kit (Solarbio, China). Images were recorded under a microscope and collagen fiber ratio was analyzed by Image.

Immunohistochemistry and Immunofluorescence Staining of Tissue Sections

For immunohistochemistry staining, the sections underwent dewaxing, hydration, and antigen retrieval procedures. Subsequently, they were incubated overnight at 4°C with anti-VEGF antibody (1:100, Abcam, ab46154). Following this incubation, the sections were exposed to HRP-conjugated secondary antibodies (1:200, Abcam) for 1 hour at room temperature. Visualization of the immunocomplexes was achieved using a DAB kit (ZSGBBIO, China).

For immunofluorescence staining, tissue sections were initially deparaffinized, rehydrated, and subjected to antigen retrieval. Following blocking, the sections were incubated overnight at 4°C with primary antibodies and their corresponding secondary antibodies as follows: anti-F4/80 (Santa Cruz, sc-25830) conjugated with Alexa Fluor 647 (Life tech, A31573), anti-CD206 (Santa Cruz, sc-58986) conjugated with Alexa Fluor 488 (Life tech, A11001), and anti-NOS2 (Santa Cruz, sc-7271) conjugated with Alexa Fluor 555 (Life tech, A21422). After PBS washing, the sections underwent nuclei counterstaining with DAPI (Sigma-Aldrich, USA) for 10 min at room temperature. Finally, following additional PBS washing, the sections were preserved with an anti-fluorescent destructor. Fluorescence imaging was performed using a confocal laser scanning microscope from Olympus, and the analysis was carried out using ImageJ software.

Statistical Analysis

The data were expressed as mean ± standard deviation (SD). To compare two groups, statistical significance was evaluated using Student's *t*-test (two-tailed). For comparisons involving multiple groups, statistical significance was determined using One-way ANOVA with Tukey's post hoc test. Significant differences between groups are indicated as * P< 0.05; ** P < 0.01; *** P < 0.001; **** P < 0.0001; NS, not significant. Statistical and graph analyses were performed using GraphPad Prism 9.4.1.

Results

Isolation and Characterization of ADSC-Derived apoSEVs

Characterization of the ADSCs utilized in this study was performed initially. The ADSCs displayed typical expression patterns of MSC surface markers, with high expression levels of CD90, CD44, and CD105, while showing negative staining for CD34, CD11b, and CD45 (Figure S1A). The ADSCs exhibited the ability to generate single colony clusters (Figure S1B) and demonstrated osteogenic and adipogenic differentiation potential when induced with osteogenic or adipogenic medium, as confirmed by alizarin red S and Oil Red O (ORO) staining, respectively (Figure S1C).

To induce apoptosis, undifferentiated ADSCs were treated with 300 nM Staurosporine (STS) for 12 hours, following established literature protocols.[31,32] Apoptotic ADSCs exhibited characteristic morphological changes such as cell rounding and shrinkage (Figure 1A and B). Flow cytometry analysis using annexin V and PI staining validated the induction of apoptosis in ADSCs (Figure 1B), which was further supported by positive TUNEL immunofluorescent staining (Figure 1C).

apoSEVs, derived from apoptotic ADSCs, were isolated using an optimized gradient centrifugation protocol (Figure 1A).[37] Transmission electron microscopy (TEM) analysis revealed that both apoSEVs and apoBDs appeared as double-membrane spherical structures. apoSEVs measured approximately 200 nm in size, while apoBDs were larger than 500 nm (Figure 1D). Nanoparticle tracking analysis (NTA) provided size distribution information for apoSEVs, demonstrating that 82.1% of ADSC-apoSEVs fell within the range of 50−300 nm (with an average size of 185.2 ± 17.7 nm) (Figure 1E). Western blot analysis confirmed the presence of apoptotic EV-specific marker, cleaved caspase-3, in apoSEVs (Figure 1F). These findings confirm that the apoSEVs utilized in this study exhibit the characteristic features of apoptotic EVs.

Notably, the quantity of apoSEV particles and protein produced by ADSCs undergoing apoptosis was significantly higher compared to the number of EVs secreted by normal ADSCs within 24 hours, as determined by both calculating the protein ratio of EV to cell and the particle concentration. Specifically, an equal number of ADSCs generated six times more apoSEV particles and four times more protein than normal EVs within a 12-hour period (Figure 1G–I). These results indicate that apoptotic cells produce a greater quantity of extracellular vesicles than normal cells.

ApoSEVs Facilitate the Phenotypic Polarization of M2 Macrophages in the Context of Diabetes

After the formation of a skin wound and achievement of hemostasis, the wound enters the inflammatory phase, during which macrophage phenotypic changes play a crucial role in the transition from inflammation to proliferation.[38] In the initial stages, M1 macrophages actively contribute to promoting inflammation and eliminating pathogens and wound debris. As the repair process progresses, the population of M1 macrophages decreases, and partly transits into M2 macrophages. M2 macrophages help secrete factors and dampen inflammation that regulate the migration and proliferation of fibroblasts and endothelial cells, thereby facilitating neovascularization and wound closure.[39] However, in the context of diabetes, where the wound environment is often compromised, the conversion of M1 macrophages into M2 macrophages becomes challenging, resulting in prolonged inflammation that hinders proper wound healing.[12,39–41] Therefore, in this study, we investigated the impact of apoSEVs, apoBDs, and normal EVs on the phenotypic polarization of macrophages from M1 to M2 under high glucose conditions (Figure 2A). A concentration of 20 μg/mL was employed for all three groups of vesicles, based on relevant published literature.[21,42,43] The morphology of Raw264.7 cells changed significantly following various treatments. Raw264.7 cells stimulated with LPS exhibited a spindle and dendritic morphology (Figure S2A). LPS+apoEV-treated cells

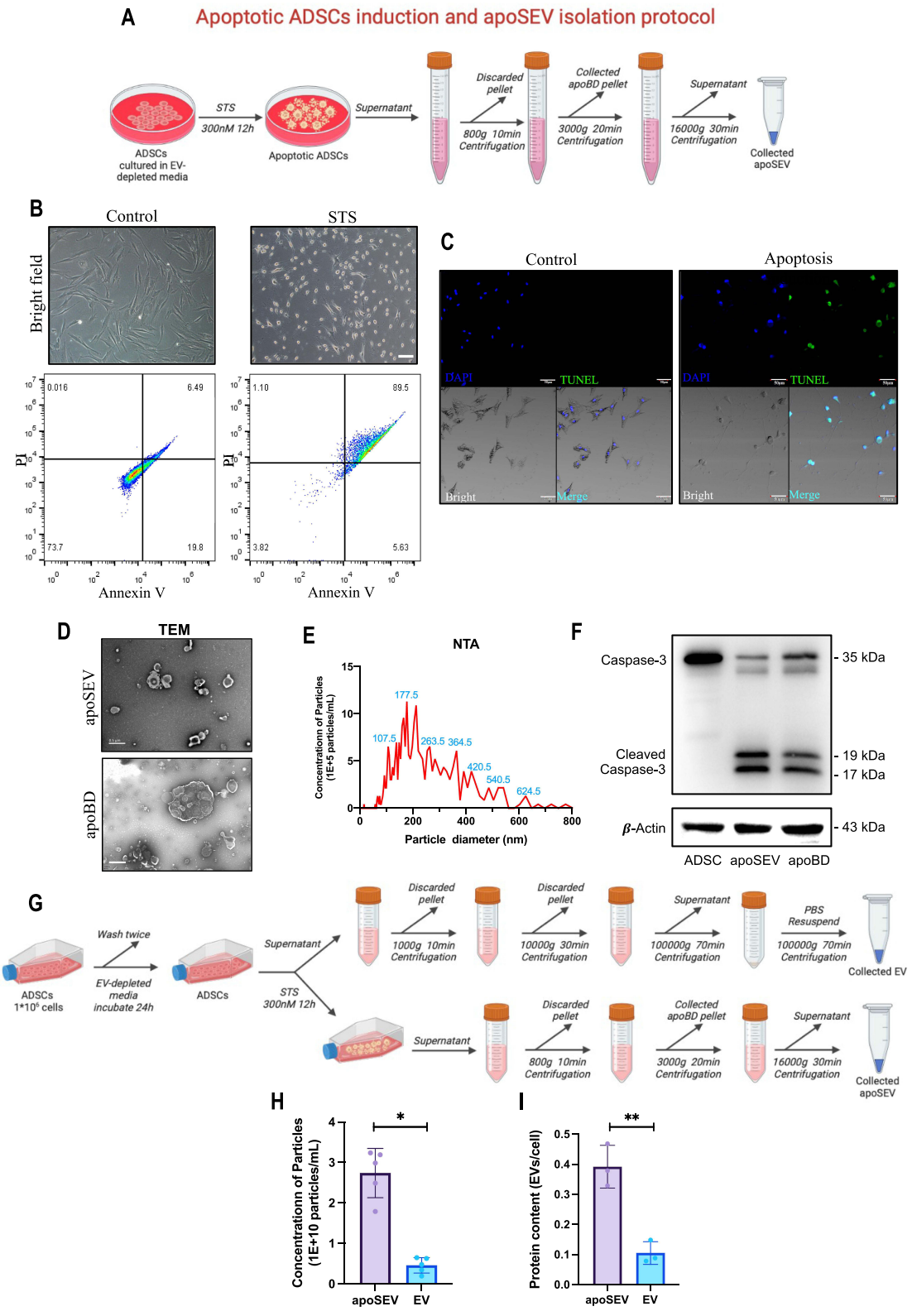

Figure 1 Apoptotic ADCSs induction and apoSEV isolation and characterization. (**A**) Schematic illustration of apoptotic ADSCs induction and apoSEV isolation. (**B** and **C**) The cellular morphology and flow cytometry analysis (**B**), and TUNEL immunofluorescent staining (**C**) of normal ADSCs and STS induced apoptosis ADSCs. Scale bar = 50 μm. (**D**) Representative image showing the morphology of apoSEV and apoBD by TEM. Scale bar = 500 nm. (**E**) The size distribution of apoSEV analyzed by NTA. (**F**) The presence of Caspase-3/Cleaved Caspase-3 in ADSC, apoSEV, and ApoBD analyzed by Western Blot. (**G**)Schematic illustration of the procedure for obtaining apoSEV and EV with the same number of ADSCs. (**H** and **I**) Quantification of the particle concentration (**H**) and the protein ratio of EV to cell (**I**). The data in the figures represent the mean ±SD. Significant differences between groups are indicated as * P< 0.05; ** P < 0.01.

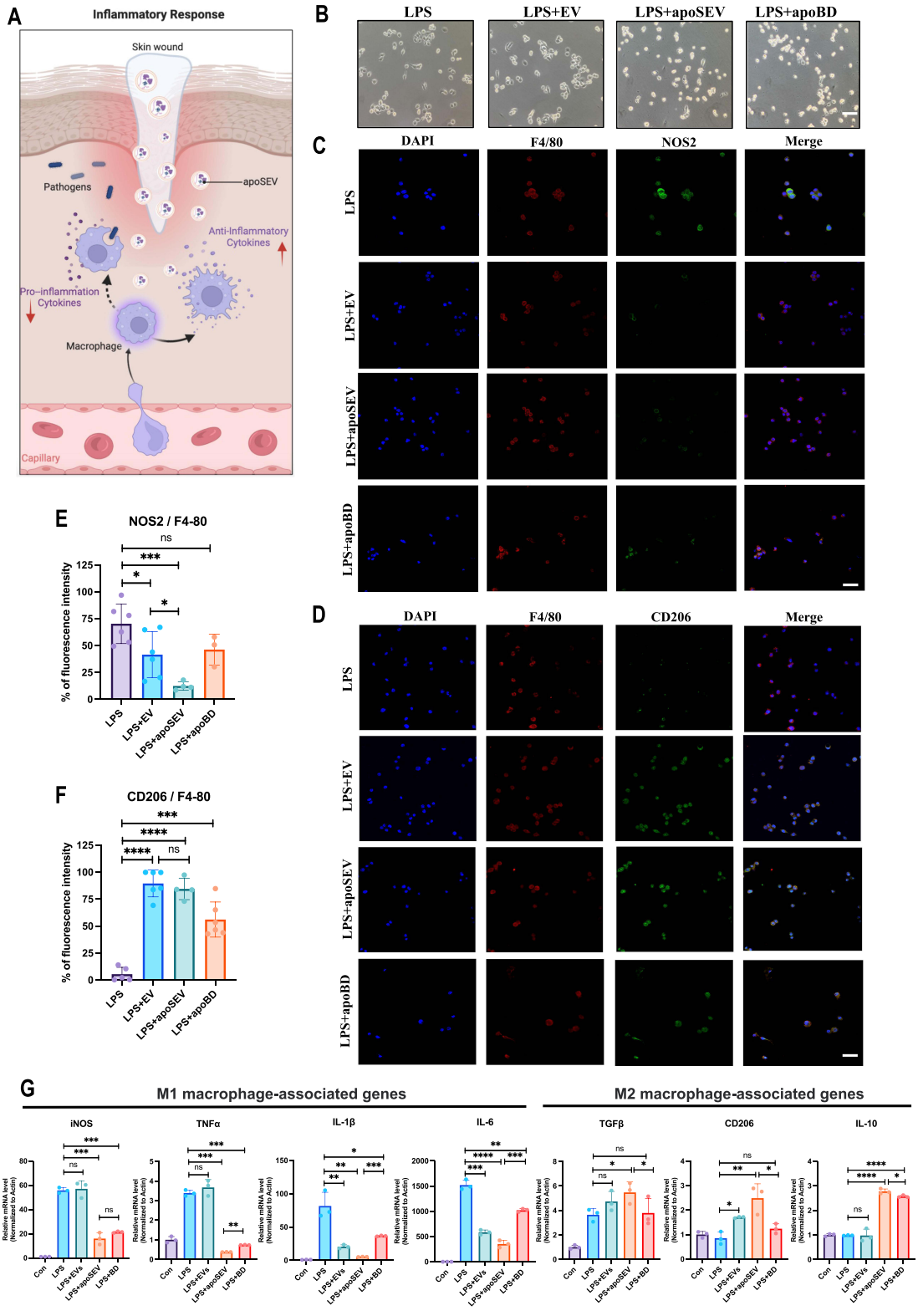

Figure 2 apoSEV inhibited the inflammatory response by increasing the ratio of M2 polarization macrophages to M1 polarization in vitro. (**A**) Schematic illustration of apoSEV promoted M2 macrophage polarization and reduced inflammation in the phase of inflammatory response. (**B**) The morphology of Raw264.7 cells treated with LPS, LPS+EV, LPS+apoSEV, and LPS+apoBD. Scale bar = 100 μm. (**C** and **D**) immunofluorescence staining of M1 macrophage marker NOS2 (**C**) and M2 macrophage marker CD206 (**D**). Scale bar = 50 μm. (**E** and **F**) Quantification of the ratio of NOS2 to F4/80 (**E**) and the ratio of CD206 to F4/80 (**F**). (**G**) The M1 and M2 macrophage relative gene expressions of iNOS, IL-1β, TNF-α, IL-6, TGFβ, CD206 and IL-10 were detected by qRT-PCR. The data in the figures represent the mean ± SD. Significant differences between groups are indicated as *P< 0.05; **P < 0.01; ***P < 0.001; ****P < 0.0001; NS, not significant.

https://doi.org/10.2147/IJN.S436350 DovePress

displayed a more spread-out morphology. LPS+apoSEV and LPS+apoBD-treated cells exhibited a rounded and shrunken morphology, with some retaining a spindle-shaped morphology (Figure 2B). Immunofluorescence results demonstrated that the expression level of the M1 marker NOS2 significantly decreased following treatment with apoSEVs and EVs, whereas the expression level of the M2 marker CD206 increased after treatment with apoSEVs, EVs, and apoBDs (Figure 2C and D). Quantitative analysis further confirmed these observations (Figure 2E and F). Subsequently, the expression levels of M1 macrophage-associated genes, including iNOS, TNFα, IL-1β, and IL-6, as well as M2 macrophage-associated genes, such as TGFβ, CD206 and IL-10, were evaluated through qRT-PCR. It was observed that the expression levels of the M1 marker gene iNOS and the pro-inflammatory cytokine TNFα, IL-1β and IL-6 significantly decreased after treatment with apoSEVs and apoBDs (Figure 2G). Regarding M2 macrophages, the marker gene TGFβ, CD206 and IL-10 showed a significant increase in expression in the apoSEV-treated groups, and only IL-10 expression was significantly increased in apoBD-treated groups (Figure 2G).

Based on the aforementioned results, it can be concluded that apoSEVs facilitated the transition of RAW264.7 macrophages towards the M2 phenotype. Moreover, the expression levels of M1 macrophage-associated genes decreased while the expression levels of M2 macrophage-associated genes increased, thereby inhibiting prolonged inflammation. Notably, apoSEVs possesses a more pronounced functional role than apoBDs.

ApoSEVs Promote the Recovery of Endothelial Cell and Fibroblast Function in the High Sugar Microenvironment

During the proliferative phase, endothelial cells and fibroblasts are recruited to the wound site to facilitate vascular regeneration and tissue repair (Figure 3A).[44,45] However, the diabetic high-glucose environment hampers the proliferation, migration, and functionality of these cells, making wound healing challenging.[11,41] Therefore, we investigated the impact of apoSEVs on endothelial and fibroblast function in vitro.

Firstly, we examined the effects of apoSEVs on the proliferation, migration, and tube formation ability of HUVECs under high glucose conditions, using EVs and apoBDs as controls. The CCK8 assay results demonstrated that apoSEVs and EVs significantly promoted HUVEC proliferation, while apoBDs slightly inhibited it (Figure 3B). For HUVEC migration, the scratch test showed that the apoSEV and EV groups achieved 44% and 35% closure, respectively, at 12 hours, while the apoBD group only reached 17% closure. After 24 hours, the scratch area of the apoSEV and EV groups was almost completely healed, whereas the apoBD group achieved only 68% closure. Similarly, the results of the transwell assay indicated that the average number of migrated cells in the apoSEV group was three times higher than that in the control group, while the apoBD group had only 0.7 times more migrated cells than the control group. These results from the scratch and transwell assays indicate that apoSEVs and EVs promote HUVEC migration, while apoBDs have an inhibitory effect (Figure 3C–G). Regarding the tube formation assay, HUVECs stimulated by apoSEVs and EVs exhibited an enhanced formation of capillary-like tubes on Matrigel compared to apoBDs and the control group (Figure 3F). Quantitative analysis of the number of branches and junctions further confirmed these observations (Figure 3H–I).

Next, we assessed the impact of apoSEVs on the proliferation and migration of human dermal fibroblasts (HDFs). The CCK8 assay revealed that apoSEVs and EVs significantly promoted cell growth compared to the control group (Figure 4A). Similar to the HUVEC proliferation assays, apoBDs inhibited the proliferative ability of HDFs. Migration of HDFs was assessed using scratch and transwell assays. In the scratch assays, the closure rates of the apoSEV and EV groups were higher than that of the control group at both 12 hours and 24 hours. At 24 hours, the closure rates of the apoSEV and EV groups reached 44% and 39%, respectively. Conversely, apoBDs exhibited an inhibitory effect, with a closure rate of only 19% at 24 hours (Figure 4B and D). In the transwell assays, a higher number of cells migrated in the apoSEV and EV groups, whereas fewer cells migrated in the apoBD group (Figure 4E). Quantitative statistical analysis indicated that apoSEVs had the most significant effect (Figure 4C).

In summary, our findings demonstrate that apoSEVs promote the recovery of fibroblast and endothelial cell functions, enhancing tube formation in the diabetic wound environment and improving the wound closure rate in diabetes mellitus. However, apoBDs did not exhibit a promoting effect and, in fact, had an opposite effect on endothelial cells and fibroblasts.

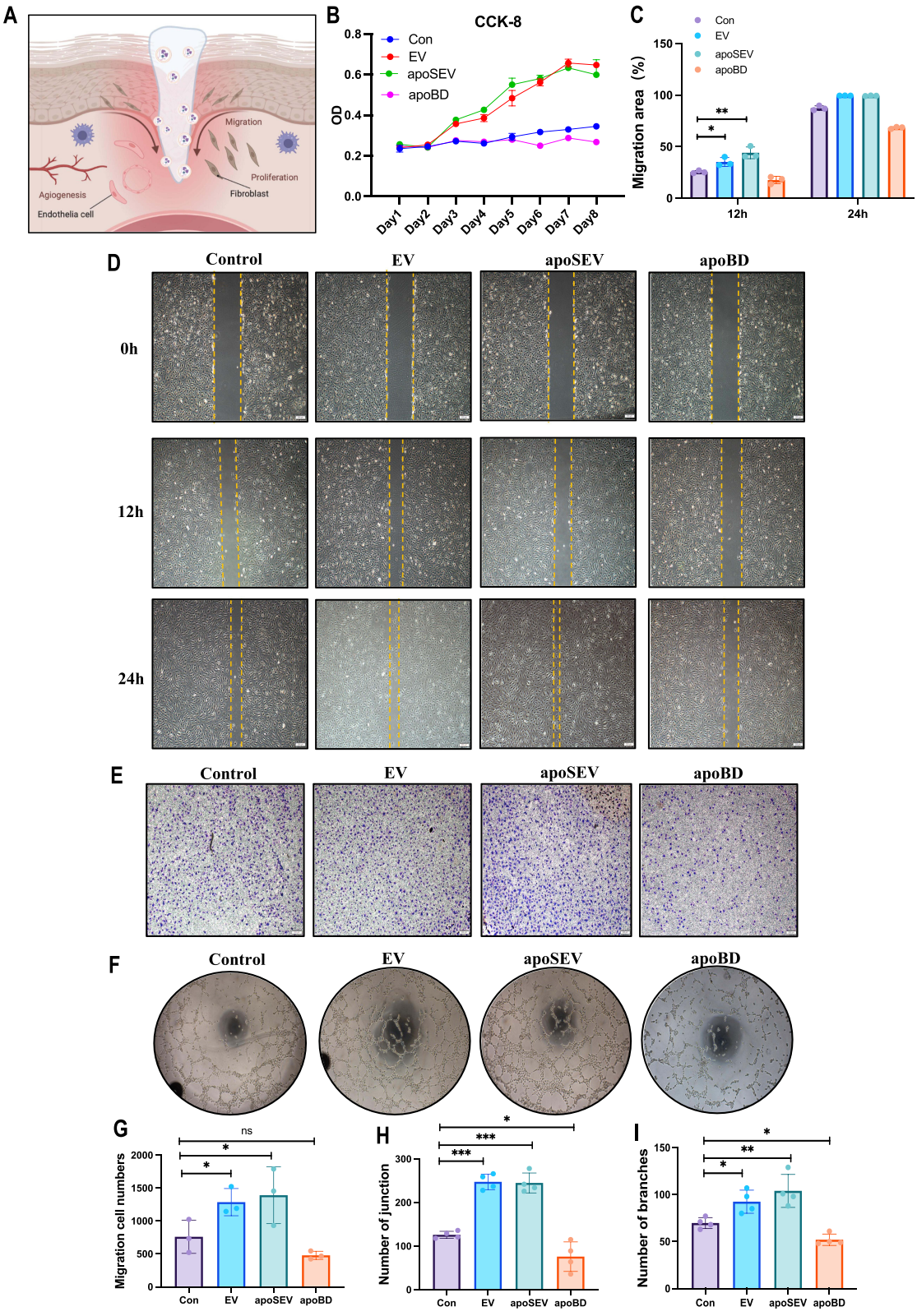

Figure 3 apoSEV promoted the proliferation, migration, and tube formation of HUVEC. (**A**) Schematic illustration of apoSEV promoted cellular function recover of the endothelia cells and fibroblast in the phase of proliferative. (**B**) The effects of apoSEV, EV and apoBD on HUVEC proliferation under high glucose conditions was examined by CCK8 assay. (**C** and **D**) Representative images showcasing the wound closure progress of HUVECs in various experimental groups, as determined through the cell scratch assay at the 12-hour and 24-hour time points (**D**). Scale bar = 200 μm. Statistical analysis of migration area (%) in scratch assay (**C**). (**E** and **G**) Representative images of transwell migration assay of HUVECs in different groups (**E**). Statistical analysis of migrated number of HUVECs in transwell assay (**G**). (**F, H** and **G**) Tube formation of HUVECs with different treatment. Scale bar = 200 μm. (**F**) Statistical analysis of total junction and branch points representing tube formation ability (**H** and **I**). The data in the figures represent the mean ±SD. Significant differences between groups are indicated as * P< 0.05; ** P < 0.01; *** P < 0.001; NS, not significant.

https://doi.org/10.2147/IJN.S436350 DovePress

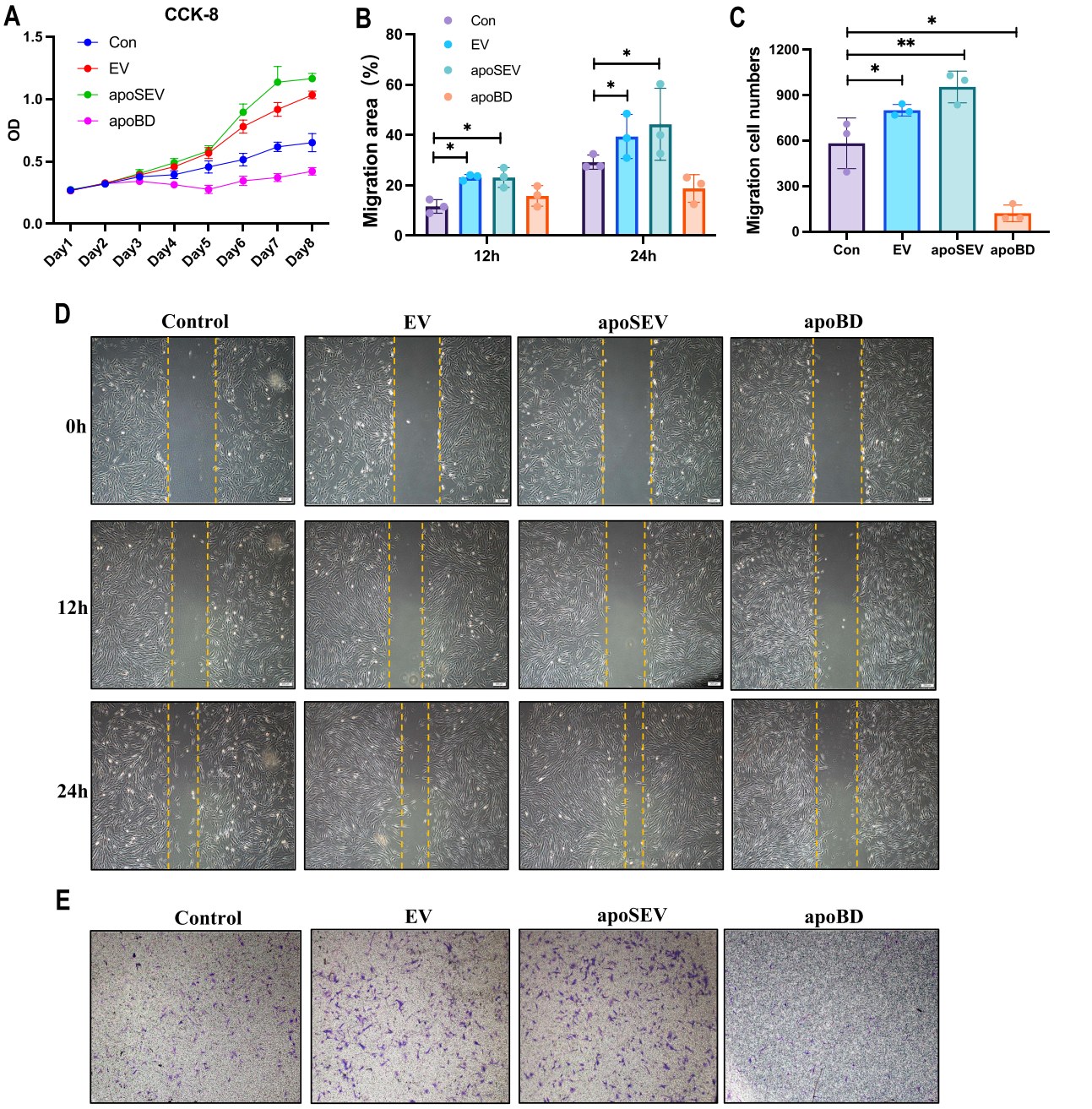

Figure 4 apoSEV promoted the proliferation and migration of HDFs. (**A**) The effects of apoSEV, EV and apoBD on HDFs proliferation under high glucose conditions was examined by CCK8 assay. (**B** and **D**) Representative images showcasing the wound closure progress of HDFs in various experimental groups, as determined through the cell scratch assay at the 12-hour and 24-hour time points (**D**). Statistical analysis of migration area (%) in scratch assay (**B**). Scale bar = 200 μm. (**E** and **C**) Representative images of transwell migration assay of HDFs in different groups (**E**). Statistical analysis of migrated number of HDFs in transwell assay (**C**). The data in the figures represent the mean ±SD. Significant differences between groups are indicated as * P< 0.05; ** P < 0.01.

GelMA Has Good Biocompatibility and Characteristics of Sustained Release of apoSEVs

Based on the aforementioned evidence, we proceeded to develop an apoSEV-based strategy for treating diabetic ulcers. Initially, we attempted to inject apoSEVs into the surrounding area of the wound. However, the use of an injection needle resulted in local skin impairment in diabetic mice. Therefore, we explored the construction of a coating that could carry apoSEVs.

GelMA, with its excellent biocompatibility and porous structure, coupled with the ease of photocatalytic coagulation, allows for its application in the storage and continuous release of cells and extracellular vesicles.[46–48] Published research

has reported that the biocompatibility, degradation, and micropore diameter of the photo-crosslinked material decrease with a higher substitution of MA and concentration.[49] To determine a suitable GelMA concentration as a carrier for vesicles in wound dressings, we selected three different concentrations: 5%, 10%, and 15%, and examined their mechanical properties and biocompatibility. Considering wound application characteristics, we focused on the deformation, degradation, biocompatible toxicity of GelMA, and its ability to sustainably release vesicles. The internal porous structure of GelMA with different concentrations was visually observed using SEM (Figure 5A). As the concentration increased, the mean pore size decreased significantly (Figure 5B). The storage and loss modulus, determined through the detection of G' and G", respectively, confirmed the gel-like nature of GelMA, with G' higher than G" for all three concentrations (Figure 5C). After 24 hours of immersion in PBS, the swelling behavior of GelMA with different concentrations increased as the concentration decreased. The swelling and deformation rates of 5%, 10%, and 15% GelMA over 24 hours were 28.65%, 20.56%, and 11.25%, respectively (Figure 5D). For wound application, GelMA in a moist environment should experience minimal deformation and swelling to fit the wound. Among the concentrations tested, 10% GelMA exhibited better deformation resistance. The degradation rate of GelMA was assessed by soaking different concentrations in saline containing collagenase and measuring the residual mass after 24 hours. The residual mass percentages of 5%, 10%, and 15% GelMA were 29.36%, 57.48%, and 80.22%, respectively (Figure 5E). The 10% GelMA concentration degraded approximately half within 24 hours. The degradation rate of 5% GelMA was much faster than that of the 10% group, while 15% GelMA exhibited the slowest degradation. Considering GelMA as a carrier for sustained vesicle release, a moderate degradation rate is necessary for achieving long-term release. The degradation rate of 5% GelMA was too fast, preventing long-term release, whereas the slow degradation of 15% GelMA would hinder the wound healing process. Thus, the degradation rate of the 10% GelMA concentration was found to be more suitable.

Next, we assessed the biocompatibility of GelMA with various concentrations on cells. We co-cultured HFDs with different concentrations of GelMA and measured cell proliferation over seven consecutive days. The results indicated that GelMA at various concentrations did not affect cell proliferation and showed no toxicity, confirming its good biocompatibility (Figure 5F). Based on the results of deformation, degradation, and biocompatibility, we concluded that 10% GelMA exhibited a moderate degradation rate and swelling deformation while showing no cytotoxicity. Therefore, we selected 10% GelMA as the optimal concentration for subsequent applications.

Subsequently, we mixed PKH26-labeled apoSEV with 10% GelMA and examined its 3D structure using fluorescence microscopy after photo-crosslinking. The 3D reconstruction images revealed the uniform distribution of apoSEV within the GelMA scaffold (Figure 5G). To further validate the sustained release effect of GelMA on apoSEVs, we co-cultured PKH26-labeled apoSEVs with HDFs in both free form and GelMA-loaded form for 12h, 24h, 48h, and 72h, respectively. We then observed the number of apoSEVs engulfed by the cells at different time points. The results demonstrated that the highest amount of apoSEV in the free form was observed at 12h, which gradually decreased over time, with almost no apoSEVs remaining at 72h. Conversely, the number of apoSEVs carried by GelMA exhibited an increasing trend, with the amount of apoSEVs rising over time and reaching its peak at 48h. Even at 72h, some apoSEVs were still present. These findings clearly demonstrate that GelMA-encapsulated apoSEVs can provide a sustained release effect (Figure 5H).

In summary, the aforementioned results indicate that 10% GelMA exhibits moderate swelling and deformation properties, along with a sustained degradation rate and good biocompatibility. The hybrid hydrogel constructed using 10% GelMA and apoSEVs enables the continuous release of vesicles, thus holding significant potential for various applications.

Treatment of apoSEVs Accelerates Diabetic Wound Healing

The aforementioned results confirm that apoSEVs can restore cellular functions of macrophages, endothelial cells, and fibroblasts in vitro. To further explore the effect of apoSEVs on skin healing in vivo, we applied dressings made from apoSEVs and GelMA to a full-thickness skin defect model in type 2 diabetic mice. Based on the in vitro results, which indicated that apoSEVs and EVs had a positive effect on cellular function recovery, while apoBDs had an inhibitory effect, we selected only apoSEVs and EVs for the in vivo study. Additionally, considering the characterization results of GelMA material, we determined that a 10% concentration would be used for the in vivo application.

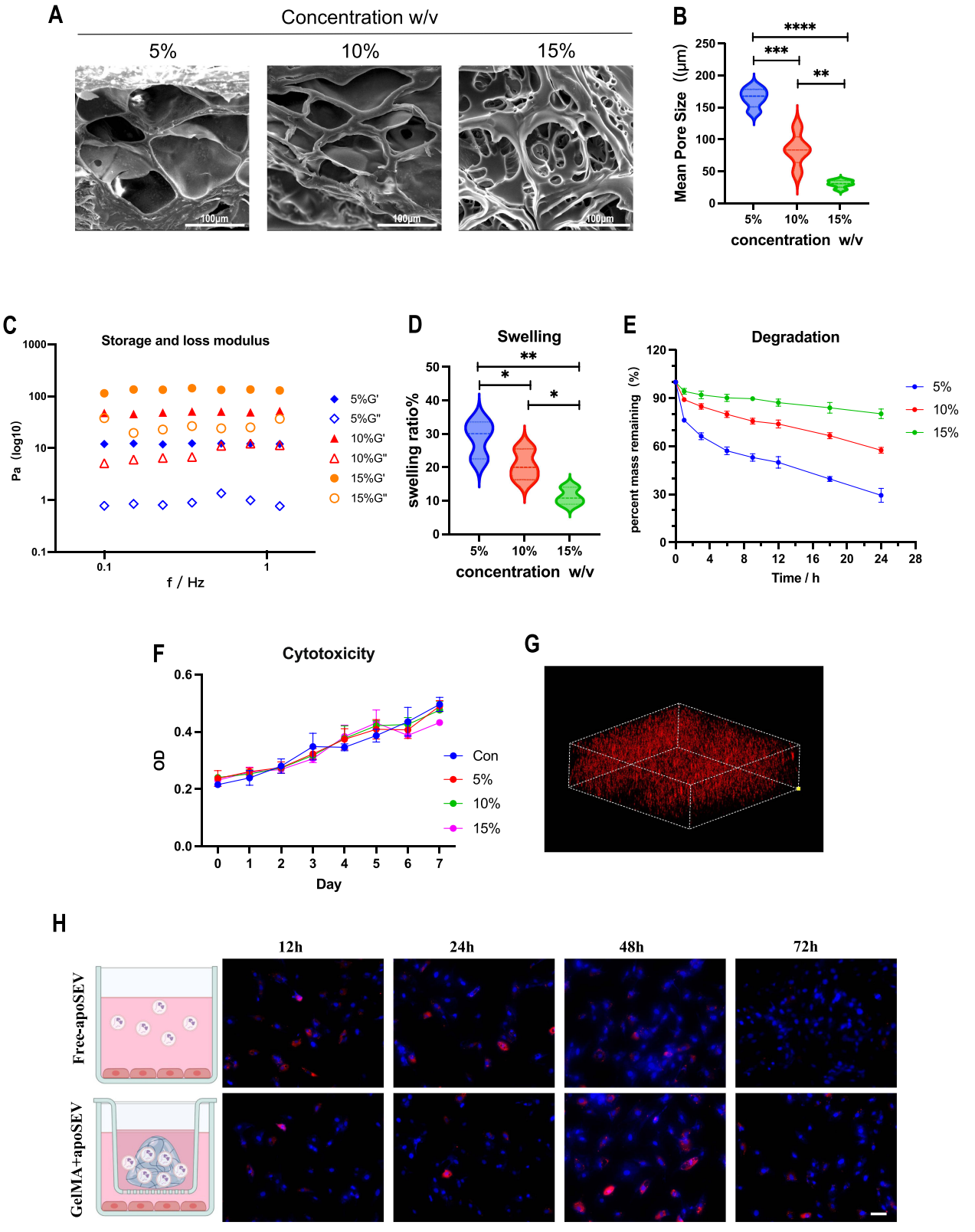

Figure 5 Characterization of GelMA and GelMA+apoSEV hydrogel. (**A**) The representative SEM images of GelMA hydrogels at different concentrations. Scale bar = 100 μm. (**B**) Mean pore size of the GelMA hydrogels at different concentration. (**C**) Storage and loss modulus of the GelMA hydrogels at different concentration. (**D**) Swelling ratio of the GelMA hydrogels at different concentration. (**E**) Degradation ratio of the GelMA hydrogels at different concentration. (**F**) Cytotoxicity of the GelMA hydrogels tested by CCK8. (**G**) Reconstruction 3D image illustrating 10% photo-crosslinked GelMA hydrogels containing apoSEVs labeled with PKH26. Scale bar = 100 μm. (**H**) Representative confocal images display HDFs co-cultured with PKH26 labeled apoSEVs (red) in both their free form and GelMA-incorporated form, with nuclei stained using DAPI (blue). Scale bar = 50 μm. The data represent the mean ±SD in the figures. Significant differences between groups are indicated as * P< 0.05; ** P < 0.01; *** P < 0.001; **** P < 0.0001.

Full-thickness skin defect wounds were created on the backs of BKS-DB mice and divided randomly into four treatment groups: Control, GelMA, GelMA+EV, and GelMA+apoSEV. The wound area of each group was recorded and measured at 0, 4, 7, 10, and 14 days (Figure 6A). To visualize the wound healing process for each group, the wound healing areas at different time points were separately displayed and overlapped (Figure 6B). From Figure 6A, it can be observed that on day 14, the skin wounds in the GelMA group and Control group, which received no treatment, were still not healed. However, the wounds in the GelMA+apoSEV and GelMA+EV treatment groups showed signs of healing. The overlapping plot in Figure 6B visually demonstrates that GelMA+apoSEV significantly accelerated wound healing (Figure 6C). These results indicate that apoSEVs have a significant promoting effect on wound healing.

H&E images revealed full-thickness regeneration and re-epithelialization of skin wounds in the defect sites of the GelMA+apoSEV and GelMA+EV groups. Zoomed images showed that at the junction of normal and defect skin sites, the epithelium was disrupted in the Control group and GelMA group, with the central area of the defect still incomplete (Figure 7A). Masson staining results demonstrated that the GelMA+apoSEV and GelMA+EV groups had a greater abundance of thicker collagen with densely arranged and better-deposited collagen fibers, while the Control group and GelMA group exhibited less collagen (Figure 7B). Quantitative analysis indicated that the GelMA+apoSEV group had a significantly higher proportion of deposited collagen fibers in the wound area compared to other groups (Figure 7E).

Angiogenesis was assessed by immunofluorescence staining for CD31, a transmembrane protein expressed during early angiogenesis, indicating neovascularization.[50,51] The fluorescence results showed the presence of more linear vessel structures in the dermis of the GelMA+apoSEV and GelMA+EV groups, with some vessels showing stained blood cells, indicating blood perfusion (Figure 7D). Quantitative analysis demonstrated that the GelMA+apoSEV and GelMA+EV groups had a larger fluorescence area compared to the other groups (Figure 7F). Furthermore, immunohistochemical staining revealed that the expression of VEGF, produced by M2 macrophages and stromal cells and effective in promoting angiogenesis, was significantly higher in the GelMA+apoSEV and GelMA+EV groups compared to other groups (Figure 7C).

Lastly, we employed immunofluorescence staining to analyze the different phenotypes of macrophages in each group. The immunofluorescence results revealed a significant decrease in the number of M1 macrophages, indicated by the NOS2 marker, within the regenerated tissues of the GelMA+apoSEV and GelMA+EV groups (Figure 8A–D). Conversely, the number of M2 macrophages, marked by CD206, showed an increase in these groups. In addition, the GelMA+apoSEV group showed decreased intensity of F4/80 in the wound area in the wound healing area, which means a decrease in macrophages infiltration. These findings indicate a favorable phenotype conducive to promoting wound healing. In contrast, the Control group and GelMA group exhibited a higher number of M1 macrophages and a lower number of M2 macrophages, which are less conducive to wound healing (Figure 8A–D).

Collectively, these data strongly suggest that GelMA coating carrying apoSEV can significantly promote the polarization of M2 macrophages, enhance angiogenesis, and facilitate collagen fiber deposition. Ultimately, this mechanism accelerates the healing of skin wounds.

Discussion

The skin serves as the natural protective layer of the human body, yet it is also highly susceptible to damage. Normally, the healing process of skin wounds involves distinct but interconnected phases, including hemostasis, inflammation, proliferation, and remodeling. However, in the presence of diabetes, the elevated glucose environment disrupts these processes, resulting in prolonged and challenging healing.[52,53] While various innovative wound repair methods have been proposed, such as local negative pressure, growth factors, and autologous platelet-rich gel, these approaches primarily create a conducive environment for skin repair without addressing the fundamental issues related to cell regeneration and repair. Recently, a pilot case-control interventional study using autologous extracellular vesicles to treat chronic venous ulcers unresponsive to conventional treatments has been published. The study's findings have significant implications for improving the treatment outcomes and quality of life for patients with chronic venous ulcers.[54] The underlying cause of impaired healing in diabetic chronic wounds stems from the high glucose environment, which triggers excessive inflammation in macrophages, reduces the proliferation and migration capacity of endothelial cells and fibroblasts, and impairs the angiogenesis ability of endothelial cells. Thus, restoring the function of these crucial cells becomes the key to

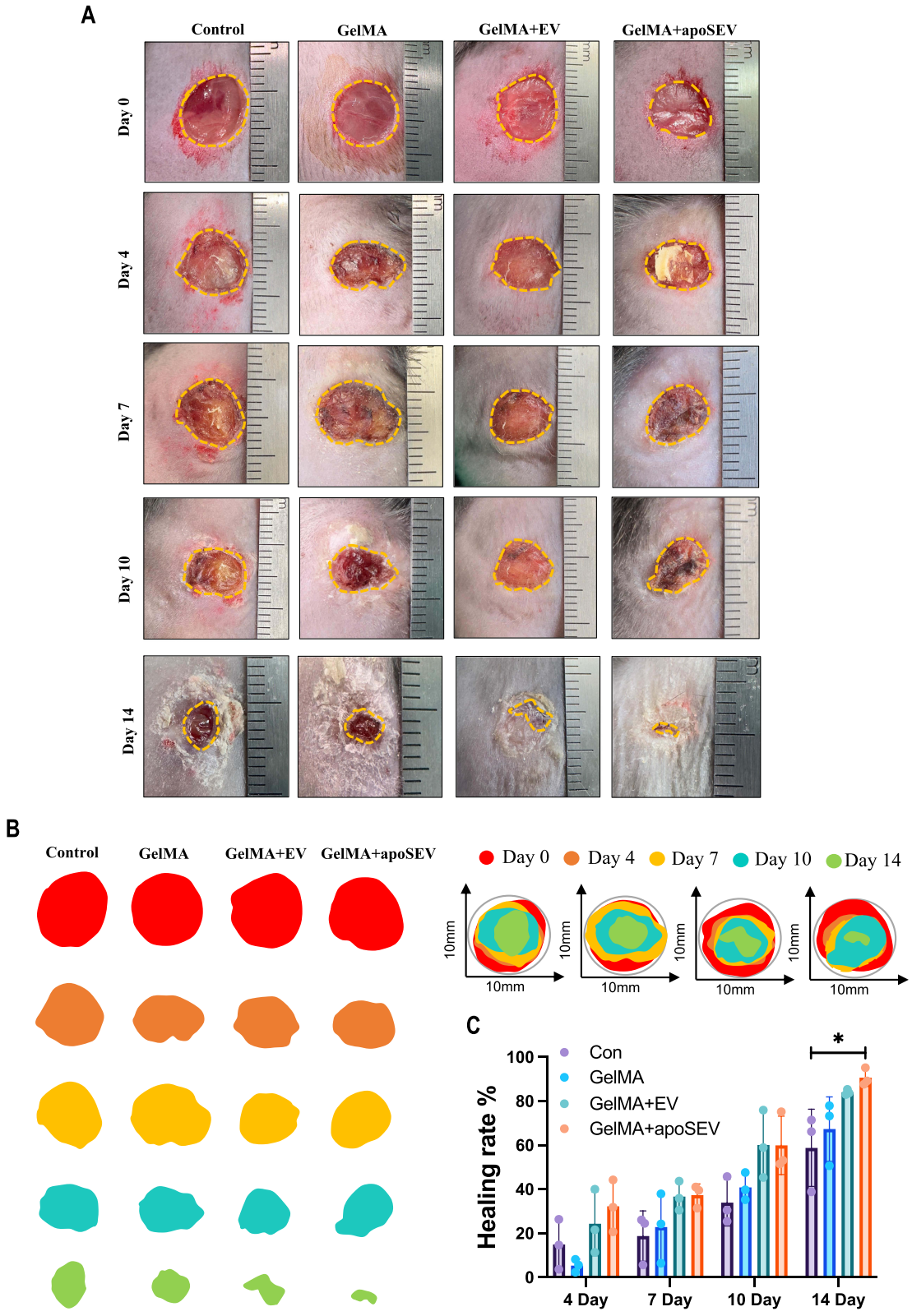

Figure 6 ApoSEV accelerates the rate of wound healing in vivo. (**A**) The gross view of wounds closure of Control, GelMA, GelMA+EV and GelMA+apoSEVs groups at day 0, 4, 7, 10 and 14. (**B**) Simulation plots of the wound closure areas at different time points and overlapped visualization groups. (**C**) Quantitative evaluation of the wound closure rate.The data represent the mean ±SD in the figures. Significant differences between groups are indicated as * P< 0.05.

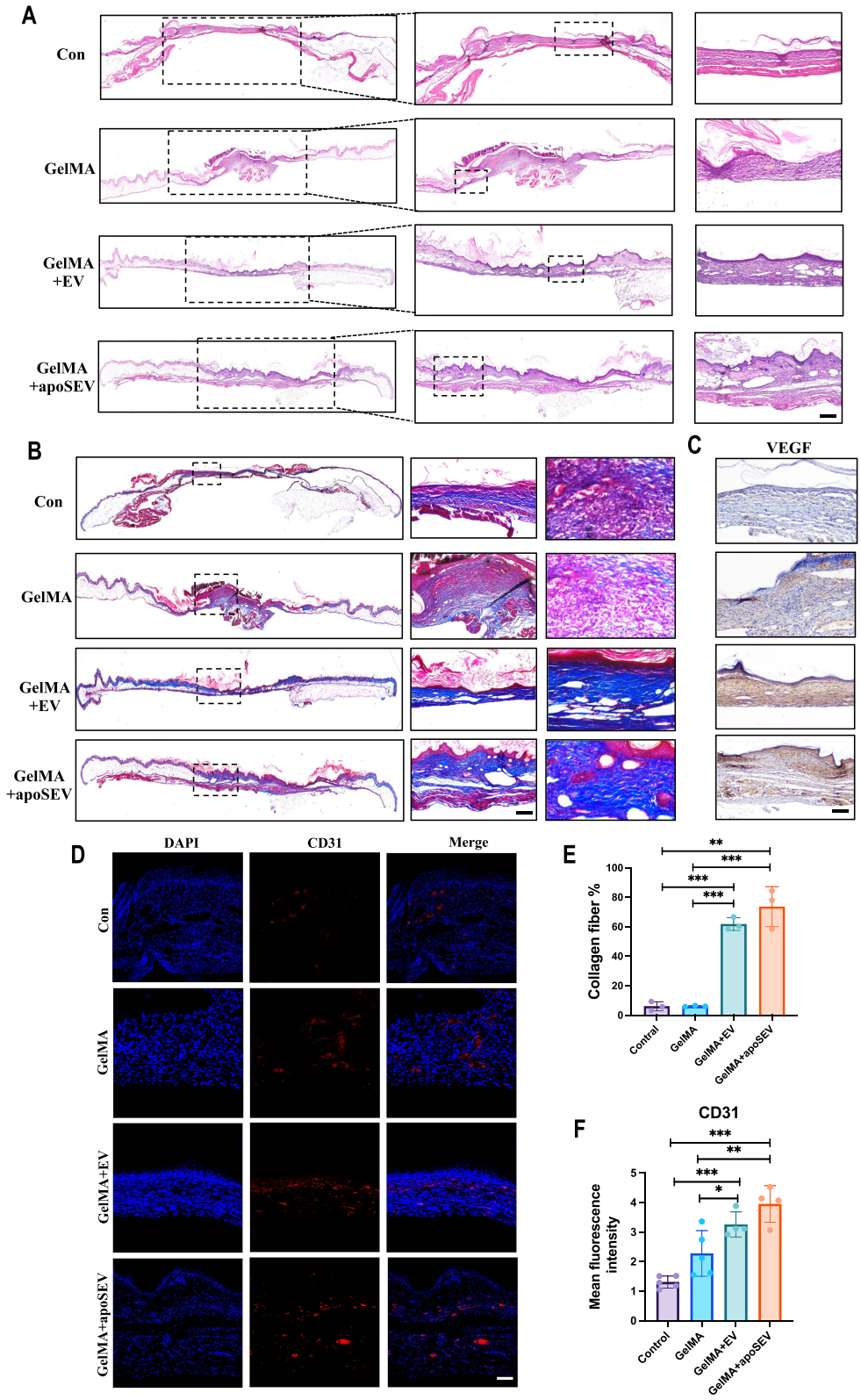

Figure 7 ApoSEV promotes wound healing and angiogenesis. (**A**) H&E staining of regenerated skin tissue in Control, GelMA, GelMA+EV and GelMA+apoSEV groups at day 14. Scale bar = 100 μm. (**B**) Masson staining of regenerated skin wounds in different groups at day 14. Scale bar = 100 μm. (**C**) Immunohistochemical staining of VEGF in regenerated skin tissue in different groups at day 14. (**D**) immunofluorescence staining of CD31 in regenerated skin tissue in different groups at day 14. Scale bar = 100 μm. (**E**) Quantitative analysis of collagen ratios of Masson staining of regenerated skin wounds in different groups at day 14. (**F**) The quantitative analysis of the relative mean density of immunohistochemical staining for CD31 in regenerated skin tissue among various experimental groups on day 14. The data represent the mean ±SD in the figures. Significant differences between groups are indicated as * P< 0.05; ** P < 0.01; *** P < 0.001.

https://doi.org/10.2147/IJN.S436350 DovePress

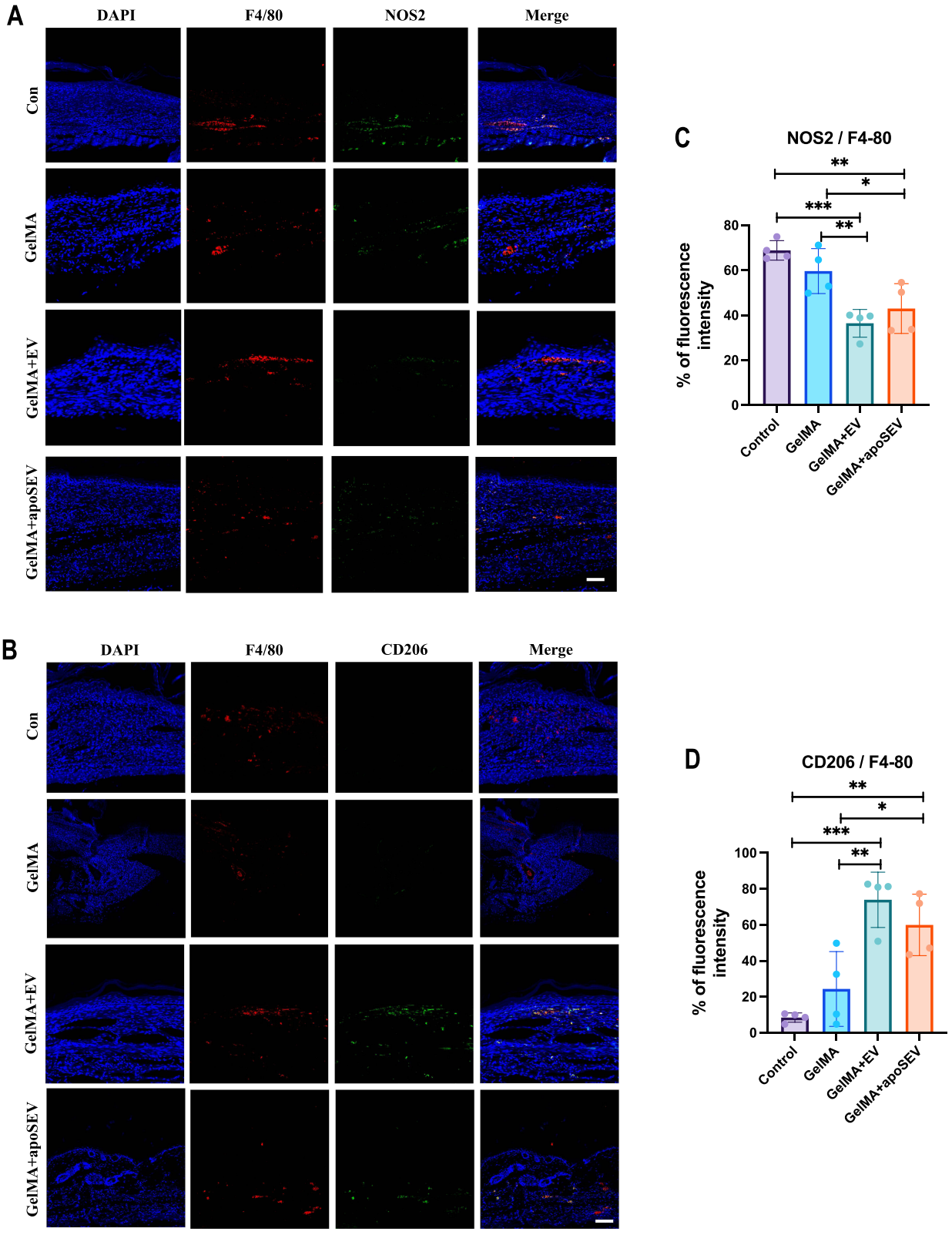

Figure 8 ApoSEV promoted an increase in the ratio of M2 polarization macrophages to M1 polarization in vivo. (**A** and **B**) immunofluorescence staining of M1 macrophage marker NOS2 (**C**) and M2 macrophage marker CD206 in regenerated skin tissue in different groups at day 14. Scale bar = 100 μm. (**C** and **D**) Quantitative analysis the ratio of relative mean density of immunohistochemical staining of NOS2 and CD206 to F4/80 in regenerated skin tissue among various experimental groups on day 14. The data represent the mean ±SD in the figures. Significant differences between groups are indicated as * P< 0.05; ** P < 0.01; *** P < 0.001.

resolving the challenge of refractory wound healing. In this study, we employed adipose-derived stem cells (ADSCs) to induce apoptosis and isolate apoSEVs. ADSCs can be obtained in ample quantities through minimally invasive procedures such as liposuction and exhibit low mortality rates and high MSC yields.[55,56] Compared to bone marrow-derived MSCs (BMSCs), ADSCs possess greater cell division capacity, making them well-suited for chronic and persistent diseases.[57] ADSCs have shown potential in enhancing the wound healing process and appear to have fewer limitations for clinical applications in skin wound healing.[58–60] Our results demonstrated that apoSEVs derived from ADSCs can promote the expression of the anti-inflammatory phenotype in macrophages, restore the proliferation and migration of endothelial cells and fibroblasts, and reinstate the tube formation capability of endothelial cells in vitro.

It is widely acknowledged that after transplantation, MSCs exhibit self-renewal and directed differentiation by homing to the site of injury, while promoting tissue repair through the secretion of EVs and soluble factors. Numerous studies have confirmed the ability of MSC-derived EVs to enhance skin healing and facilitate tissue regeneration and repair in various contexts.[11,16,61–63] However, despite these findings, the precise mechanisms by which MSCs exert their therapeutic effects remain to be fully elucidated.[64] Notably, since apoptosis occurs rapidly in transplanted MSCs in vivo, it is crucial to understand the mechanisms underlying MSC-mediated therapeutic effects. Apoptosis, as a primary form of programmed cell death, is recognized as a physiological process that plays a vital role in development, tissue homeostasis, aging, and pathogenesis.[65–67] The delicate balance between stem cell-mediated efforts, including compensatory proliferation, and the apoptosis of neighboring stem or somatic cells is indispensable for tissue regeneration following injury.[68] Studies have reported that WNT and c-Jun amino-terminal kinase (JNK) signaling pathways, triggered by surrounding apoptotic stimuli, contribute to compensatory proliferation.[69] In the context of MSC transplantation, apoptosis has also garnered significant attention as an important biological process. For instance, it has been observed that infused human MSCs become trapped and disappear in the lung, while the upregulation of the anti-inflammatory protein TSG-6 in the lung helps prevent injury.[70] Given the importance of MSC apoptosis after transplantation, further elucidation of the apoptotic mechanisms involved in MSCs and the effects and mechanisms of apoEVs secreted by apoptotic MSCs will enhance our understanding of apoptosis-mediated MSC transplantation, shedding light on the potential of apoEVs as cell-free therapeutics.

Apoptotic extracellular vesicles (apoEVs) encompass two distinct subpopulations, namely apoBDs and apoSEVs, with particle sizes ranging from 1–5 μm and 0.1–1 μm, respectively. To the best of our knowledge, the production and secretion mechanisms of apoEVs share similarities with EVs but are characterized specifically by the involvement of apoptosis.[29,71,72] The generation of apoEVs is largely regulated by the apoptotic process, as further supported by evidence showing Caspase 3 as an upstream molecule for apoEV formation.[73] During apoptosis, the cell membrane undergoes shrinkage and invagination, leading to the formation of vesicular bodies that ultimately give rise to apoptotic bodies through germination and abscission mechanisms.[71] Additionally, apoEVs include a subset of exosome-like particles that are initially formed within intracellular multivesicular bodies (MVBs). However, the molecular pathway involved in apoEV release exhibits distinctive features. While MVBs are primarily formed through plasma membrane and endosomal membrane invagination via ESCRT-dependent and -independent mechanisms, apoEVs are released through a specific molecular pathway mediated by Rab11/27/35-mediated exocytosis.[72] Different secretion patterns give rise to the formation of large vesicle apoBDs and small vesicle apoSEVs, which possess distinct soluble metabolites, thereby conferring diverse functional properties. Although limited studies have focused on comparing the characteristics of apoSEVs and apoBDs, it has been demonstrated that apoSEVs contain a more active 20S proteasome core compared to apoBDs.[74] Thus, the transfer of biological signals in the form of apoEVs may represent a unique and specific mechanism. However, further investigations are required to explore whether the differential production mechanisms of apoEVs contribute to potential functional discrepancies among apoEV subpopulations.

In line with previously published findings, our study confirmed that apoBDs have the ability to promote M2 polarization and induce an anti-inflammatory phenotype in macrophages in vitro.[21] However, we observed a suppressive effect on the proliferation and migration ability of fibroblasts and endothelial cells, which remains unexplained by the current study. Further research by our group will be conducted to investigate this phenomenon. To facilitate skin healing, we selected apoSEVs and EVs that demonstrated the ability to promote cell function recovery in vitro for further investigation in an in vivo study. Furthermore, it has been demonstrated that apoEVs can induce

transcription-level macrophage reprogramming in an efferocytosis-dependent manner, leading to the inhibition of macrophage accumulation and the transformation of macrophages towards an anti-inflammatory phenotype in T2D liver.[32] However, the specific bioactive factors carried by apoSEVs and their role in promoting the recovery and regulation of fibroblasts and endothelial cells remain unclear. To address this, proteomic analysis of apoSEVs and apoBDs will be conducted.

Meanwhile, there have been reports on the beneficial effects of EVs in promoting tissue and organ regeneration.[21,31,75] However, further confirmation is needed to determine whether apoSEVs derived from apoptotic MSCs can effectively enhance diabetic skin wound healing. Moreover, in the early stages after transplantation, it is important to determine which type of vesicle is more abundant in terms of EVs or apoSEVs produced by MSCs. With this in mind, we designed an assay to investigate this aspect in our study. We isolated EVs and apoSEVs from the same number of ADSCs and confirmed that apoSEVs were much more abundant than EVs by comparing protein ratios and particle numbers. Our additional findings also demonstrated that apoSEVs, compared to EVs, exhibited similar functions in promoting cell function recovery and tissue regeneration, and in some aspects, even showed superior effects. Therefore, it can be assumed that MSCs primarily produce apoSEVs following apoptosis after transplantation, which is the main reason why we chose apoSEVs for application in diabetic skin wound healing.

Compared to conventional EVs, apoEVs possess unique membrane molecular components, such as the apoptotic marker phosphatidylserine (PtdSer) and C1q. They also exhibit distinct miRnomes and proteomes based on specific content distribution during apoptosis.[74,76–78] These characteristics can serve as standards for the identification, isolation, and purification of apoEVs. Convenient purification and identification procedures, including gradient centrifugation and flow cytometry analysis, have been previously employed in experiments.[37] Moreover, our results from this study demonstrate that apoEVs generated by the same amount of cells yield a much higher output in a short timeframe compared to EVs produced by normal cells. Considering the high yield and larger size of apoEVs, it may be unnecessary to undergo laborious ultracentrifugation isolation steps, thereby offering a more convenient and rapid approach for the application of apoEV-based cell-free therapeutics.[75]

GelMA hydrogel has gained wide recognition as a favorable biological scaffold material. In the context of skin wound models, the unique photo-crosslinking property of GelMA makes it suitable for fusion and filling within the wound defect. However, the optimal concentration of GelMA can vary across different studies.[46,48,79] Considering its application in skin healing, the chosen GelMA concentration should meet several basic requirements, including resistance to deformation, slow degradation over a period of time with continuous vesicle release, and the ability to support skin growth and healing. In our preliminary experiment, we constructed a skin defect model in normal mice and treated the wounds with different concentrations of GelMA. Through comparison, we observed that 5% GelMA lacked sufficient strength and was prone to deformation and destruction, while 15% GelMA was excessively rigid and degraded slowly, hindering skin wound healing. However, 10% GelMA demonstrated a moderate condition, providing suitable strength without easy destruction, along with a moderate degradation rate. Therefore, considering these comprehensive factors, we selected 10% GelMA for the purpose of wound healing in our experiment.

Another important aspect to discuss is the impact of scabs on wound healing rate observed in our in vivo study. Throughout the recording process of wound healing, scabs gradually formed before the 10th day, and no significant differences were observed between the groups during this period. However, between days 10 and 14, after the scab fell off, we observed remarkable differences in the speed and progression of skin healing, as indicated by our results. We hypothesize that scabs might hinder tissue healing to some extent, potentially due to the presence of residual undegraded hydrogel. Early shedding of scabs during the middle and late stages of wound healing may have a certain effect on promoting skin healing.

Conclusion

In this study, our findings collectively demonstrate the significant ability of apoSEVs derived from ADSCs to enhance cellular function recovery and promote skin wound healing in diabetic models, both in vitro and in vivo. Our results confirm the positive effects of apoSEVs on crucial cells involved in the inflammatory and proliferative phases, such as macrophages, endothelial cells, and fibroblasts, in vitro. Remarkably, the application of our novel dressing, composed of

apoSEVs and GelMA hydrogel, to an in vivo model of diabetic skin wounds showed impressive healing effects. Overall, apoSEVs treatment expands the current therapeutic strategies for diabetic skin wound healing and holds great promise as a potential therapeutic approach to expedite the healing of diabetes-related skin wounds.

Acknowledgments

This work was supported by grants from the National Key Research and Development Program of China (2021YFA1100603), the National Natural Science Foundation of China (82071092, U21A20369), Sichuan Science and Technology Program (2023YFS0056), and the FundamentalResearch Funds for the Central Universities (SCU2023D014).

Author Contributions

All authors made a significant contribution to the work reported, whether that is in the conception, study design, execution, acquisition of data, analysis and interpretation, or in all these areas; took part in drafting, revising or critically reviewing the article; gave final approval of the version to be published; have agreed on the journal to which the article has been submitted; and agree to be accountable for all aspects of the work.

Disclosure

The authors report no conflicts of interest in this work.

References

1. Chen L, Gao Y, Li Y, et al. Severe intermittent hypoxia modulates the macrophage phenotype and impairs wound healing through downregulation of HIF-2α. *Nat Sci Sleep*. 2022;14:1511–1520. doi:10.2147/NSS.S382275
2. Patel S, Srivastava S, Singh MR, Singh D. Mechanistic insight into diabetic wounds: pathogenesis, molecular targets and treatment strategies to pace wound healing. *Biomed Pharmacother*. 2019;112:108615. doi:10.1016/j.biopha.2019.108615
3. Lim JZ, Ng NS, Thomas C. Prevention and treatment of diabetic foot ulcers. *J R Soc Med*. 2017;110(3):104–109. doi:10.1177/0141076816688346
4. Bowling FL, Rashid ST, Boulton AJ. Preventing and treating foot complications associated with diabetes mellitus. *Nat Rev Endocrinol*. 2015;11(10):606–616. doi:10.1038/nrendo.2015.130
5. Kerr M, Rayman G, Jeffcoate WJ. Cost of diabetic foot disease to the National Health Service in England. *Diabet Med*. 2014;31(12):1498–1504. doi:10.1111/dme.12545
6. Grennan D. Diabetic Foot Ulcers. *JAMA*. 2019;321(1):114. doi:10.1001/jama.2018.18323
7. Chen L, Sun S, Gao Y, Ran X. Global mortality of diabetic foot ulcer: a systematic review and meta-analysis of observational studies. *Diabetes Obes Metab*. 2023;25(1):36–45. doi:10.1111/dom.14840
8. Everett E, Mathioudakis N. Update on management of diabetic foot ulcers. *Ann N Y Acad Sci*. 2018;1411(1):153–165. doi:10.1111/nyas.13569
9. Powers JG, Higham C, Broussard K, Phillips TJ. Wound healing and treating wounds: chronic wound care and management. *J Am Acad Dermatol*. 2016;74(4):607–625; quiz 625–606. doi:10.1016/j.jaad.2015.08.070
10. Broughton G, Janis JE, Attinger CE. The basic science of wound healing. *Plast Reconstr Surg*. 2006;117(7 Suppl):12s–34s. doi:10.1097/01.prs.0000225430.42531.c2
11. Li D, Wu N. Mechanism and application of exosomes in the wound healing process in diabetes mellitus. *Diabetes Res Clin Pract*. 2022;187:109882. doi:10.1016/j.diabres.2022.109882
12. Louiselle AE, Niemiec SM, Zgheib C, Liechty KW. Macrophage polarization and diabetic wound healing. *Transl Res*. 2021;236:109–116. doi:10.1016/j.trsl.2021.05.006
13. Kaur R, Kaur M, Singh J. Endothelial dysfunction and platelet hyperactivity in type 2 diabetes mellitus: molecular insights and therapeutic strategies. *Cardiovasc Diabetol*. 2018;17(1):121. doi:10.1186/s12933-018-0763-3
14. Lopes L, Setia O, Aurshina A, et al. Stem cell therapy for diabetic foot ulcers: a review of preclinical and clinical research. *Stem Cell Res Ther*. 2018;9(1):188. doi:10.1186/s13287-018-0938-6
15. Kanji S, Das H. Advances of stem cell therapeutics in cutaneous wound healing and regeneration. *Mediators Inflamm*. 2017;2017:5217967. doi:10.1155/2017/5217967
16. Zhu LP, Tian T, Wang JY, et al. Hypoxia-elicited mesenchymal stem cell-derived exosomes facilitates cardiac repair through miR-125b-mediated prevention of cell death in myocardial infarction. *Theranostics*. 2018;8(22):6163–6177. doi:10.7150/thno.28021
17. Eirin A, Zhu XY, Puranik AS, et al. Mesenchymal stem cell-derived extracellular vesicles attenuate kidney inflammation. *Kidney Int*. 2017;92(1):114–124. doi:10.1016/j.kint.2016.12.023
18. Zhu YG, Feng XM, Abbott J, et al. Human mesenchymal stem cell microvesicles for treatment of Escherichia coli endotoxin-induced acute lung injury in mice. *Stem Cells*. 2014;32(1):116–125. doi:10.1002/stem.1504
19. Shigemoto-Kuroda T, Oh JY, Kim DK, et al. MSC-derived extracellular vesicles attenuate immune responses in two autoimmune murine models: type 1 diabetes and uveoretinitis. *Stem Cell Rep*. 2017;8(5):1214–1225. doi:10.1016/j.stemcr.2017.04.008
20. Kfoury Y, Scadden DT. Mesenchymal cell contributions to the stem cell niche. *Cell Stem Cell*. 2015;16(3):239–253. doi:10.1016/j.stem.2015.02.019

21. Liu J, Qiu X, Lv Y, et al. Apoptotic bodies derived from mesenchymal stem cells promote cutaneous wound healing via regulating the functions of macrophages. *Stem Cell Res Ther*. 2020;11(1):507. doi:10.1186/s13287-020-02014-w
22. Liu S, Jiang L, Li H, et al. Mesenchymal stem cells prevent hypertrophic scar formation via inflammatory regulation when undergoing apoptosis. *J Invest Dermatol*. 2014;134(10):2648–2657. doi:10.1038/jid.2014.169
23. Liu H, Liu S, Qiu X, et al. Donor MSCs release apoptotic bodies to improve myocardial infarction via autophagy regulation in recipient cells. *Autophagy*. 2020;16(12):2140–2155. doi:10.1080/15548627.2020.1717128
24. Green DR. The coming decade of cell death research: five riddles. *Cell*. 2019;177(5):1094–1107. doi:10.1016/j.cell.2019.04.024
25. Nagata S. Apoptosis and clearance of apoptotic cells. *Annu Rev Immunol*. 2018;36:489–517. doi:10.1146/annurev-immunol-042617-053010
26. Elliott MR, Ravichandran KS. The dynamics of apoptotic cell clearance. *Dev Cell*. 2016;38(2):147–160. doi:10.1016/j.devcel.2016.06.029
27. Kerr JF, Wyllie AH, Currie AR. Apoptosis: a basic biological phenomenon with wide-ranging implications in tissue kinetics. *Br J Cancer*. 1972;26(4):239–257. doi:10.1038/bjc.1972.33
28. Poon IKH, Parkes MAF, Jiang L, et al. Moving beyond size and phosphatidylserine exposure: evidence for a diversity of apoptotic cell-derived extracellular vesicles in vitro. *J Extracell Vesicles*. 2019;8(1):1608786. doi:10.1080/20013078.2019.1608786
29. Park SJ, Kim JM, Kim J, et al. Molecular mechanisms of biogenesis of apoptotic exosome-like vesicles and their roles as damage-associated molecular patterns. *Proc Natl Acad Sci U S A*. 2018;115(50):E11721–e11730. doi:10.1073/pnas.1811432115
30. Li M, Liao L, Tian W. Extracellular vesicles derived from apoptotic cells: an essential link between death and regeneration. *Front Cell Dev Biol*. 2020;8:573511. doi:10.3389/fcell.2020.573511
31. Ma L, Chen C, Liu D, et al. Apoptotic extracellular vesicles are metabolized regulators nurturing the skin and hair. *Bioact Mater*. 2023;19:626–641. doi:10.1016/j.bioactmat.2022.04.022
32. Zheng C, Sui B, Zhang X, et al. Apoptotic vesicles restore liver macrophage homeostasis to counteract type 2 diabetes. *J Extracell Vesicles*. 2021;10(7):e12109. doi:10.1002/jev2.12109
33. Wang R, Hao M, Kou X, et al. Apoptotic vesicles ameliorate lupus and arthritis via phosphatidylserine-mediated modulation of T cell receptor signaling. *Bioact Mater*. 2023;25:472–484. doi:10.1016/j.bioactmat.2022.07.026
34. Zhang X, Tang J, Kou X, et al. Proteomic analysis of MSC-derived apoptotic vesicles identifies Fas inheritance to ameliorate haemophilia a via activating platelet functions. *J Extracell Vesicles*. 2022;11(7):e12240. doi:10.1002/jev2.12240
35. Wilson A, Chee M, Butler P, Boyd AS. Isolation and characterisation of human adipose-derived stem cells. *Methods Mol Biol*. 2019;1899:3–13.
36. Yang J, Gao X, Xing X, et al. An isolation system to collect high quality and purity extracellular vesicles from serum. *Int J Nanomedicine*. 2021;16:6681–6692. doi:10.2147/IJN.S328325
37. Chen D, Zhao Z, Zhang K, Jin F, Zheng C, Jin Y. Protocol for differential centrifugation-based separation and characterization of apoptotic vesicles derived from human mesenchymal stem cells. *STAR Protoc*. 2022;3(4):101695. doi:10.1016/j.xpro.2022.101695
38. Boniakowski AE, Kimball AS, Jacobs BN, Kunkel SL, Gallagher KA. Macrophage-mediated inflammation in normal and diabetic wound healing. *J Immunol*. 2017;199(1):17–24. doi:10.4049/jimmunol.1700223
39. Aitcheson SM, Frentiu FD, Hurn SE, Edwards K, Murray RZ. Skin wound healing: normal macrophage function and macrophage dysfunction in diabetic wounds. *Molecules*. 2021;26(16). doi:10.3390/molecules26164917
40. Bannon P, Wood S, Restivo T, Campbell L, Hardman MJ, Mace KA. Diabetes induces stable intrinsic changes to myeloid cells that contribute to chronic inflammation during wound healing in mice. *Dis Model Mech*. 2013;6(6):1434–1447. doi:10.1242/dmm.012237
41. Theocharidis G, Thomas BE, Sarkar D, et al. Single cell transcriptomic landscape of diabetic foot ulcers. *Nat Commun*. 2022;13(1):181. doi:10.1038/s41467-021-27801-8
42. Wang J, Cao Z, Wang P, et al. Apoptotic extracellular vesicles ameliorate multiple myeloma by restoring fas-mediated apoptosis. *ACS Nano*. 2021;15(9):14360–14372. doi:10.1021/acsnano.1c03517
43. Oh EJ, Gangadaran P, Rajendran RL, et al. Extracellular vesicles derived from fibroblasts promote wound healing by optimizing fibroblast and endothelial cellular functions. *Stem Cells*. 2021;39(3):266–279. doi:10.1002/stem.3310
44. Yoo SY, Kwon SM. Angiogenesis and its therapeutic opportunities. *Mediators Inflamm*. 2013;2013:127170. doi:10.1155/2013/127170
45. Suga H, Rennert RC, Rodrigues M, et al. Tracking the elusive fibrocyte: identification and characterization of collagen-producing hematopoietic lineage cells during murine wound healing. *Stem Cells*. 2014;32(5):1347–1360. doi:10.1002/stem.1648
46. Zhao D, Yu Z, Li Y, Wang Y, Li Q, Han D. GelMA combined with sustained release of HUVECs derived exosomes for promoting cutaneous wound healing and facilitating skin regeneration. *J Mol Histol*. 2020;51(3):251–263. doi:10.1007/s10735-020-09877-6
47. Wu K, He C, Wu Y, et al. Preservation of small extracellular vesicle in gelatin methacryloyl hydrogel through reduced particles aggregation for therapeutic applications. *Int J Nanomedicine*. 2021;16:7831–7846. doi:10.2147/IJN.S334194
48. Wang Y, Cao Z, Wei Q, et al. VH298-loaded extracellular vesicles released from gelatin methacryloyl hydrogel facilitate diabetic wound healing by HIF-1α-mediated enhancement of angiogenesis. *Acta Biomater*. 2022;147:342–355. doi:10.1016/j.actbio.2022.05.018
49. Yue K, Trujillo-de santiago G, Alvarez MM, Tamayol A, Annabi N, Khademhosseini A. Synthesis, properties, and biomedical applications of gelatin methacryloyl (GelMA) hydrogels. *Biomaterials*. 2015;73:254–271. doi:10.1016/j.biomaterials.2015.08.045
50. Liang C, Liang Q, Xu X, et al. Bone morphogenetic protein 7 mediates stem cells migration and angiogenesis: therapeutic potential for endogenous pulp regeneration. *Int J Oral Sci*. 2022;14(1):38. doi:10.1038/s41368-022-00188-y
51. Chen YH, Rao ZF, Liu YJ, et al. Multifunctional injectable hydrogel loaded with cerium-containing bioactive glass nanoparticles for diabetic wound healing. *Biomolecules*. 2021;11(5):702. doi:10.3390/biom11050702
52. Okonkwo UA, DiPietro LA. Diabetes and wound angiogenesis. *Int J Mol Sci*. 2017;18(7):1419. doi:10.3390/ijms18071419
53. Wilkinson HN, Hardman MJ. Wound healing: cellular mechanisms and pathological outcomes. *Open Biol*. 2020;10(9):200223. doi:10.1098/rsob.200223
54. Gibello L, D'Antico S, Salafia M, et al. First pilot case-control interventional study using autologous extracellular vesicles to treat chronic venous ulcers unresponsive to conventional treatments. *Pharmacol Res*. 2023;190:106718. doi:10.1016/j.phrs.2023.106718
55. Frese L, Dijkman PE, Hoerstrup SP. Adipose tissue-derived stem cells in regenerative medicine. *Transfus Med Hemother*. 2016;43(4):268–274. doi:10.1159/000448180
56. Domenis R, Lazzaro L, Calabrese S, et al. Adipose tissue derived stem cells: in vitro and in vivo analysis of a standard and three commercially available cell-assisted lipotransfer techniques. *Stem Cell Res Ther*. 2015;6(1):2. doi:10.1186/scrt536

57. Kokai LE, Marra K, Rubin JP. Adipose stem cells: biology and clinical applications for tissue repair and regeneration. *Transl Res*. 2014;163(4):399–408. doi:10.1016/j.trsl.2013.11.009
58. Shu W, Shu YT, Dai CY, Zhen QZ. Comparing the biological characteristics of adipose tissue-derived stem cells of different persons. *J Cell Biochem*. 2012;113(6):2020–2026. doi:10.1002/jcb.24070
59. Shingyochi Y, Orbay H, Mizuno H. Adipose-derived stem cells for wound repair and regeneration. *Expert Opin Biol Ther*. 2015;15(9):1285–1292. doi:10.1517/14712598.2015.1053867
60. Sheng L, Yang M, Liang Y, Li Q. Adipose tissue-derived stem cells (ADSCs) transplantation promotes regeneration of expanded skin using a tissue expansion model. *Wound Repair Regen*. 2013;21(5):746–754. doi:10.1111/wrr.12080
61. Xu L, Liu Y, Tang L, Xiao H, Yang Z, Wang S. Preparation of recombinant human collagen III protein hydrogels with sustained release of extracellular vesicles for skin wound healing. *Int J Mol Sci*. 2022;23(11):6289.
62. Wen B, Huang Y, Qiu T, et al. Reparative dentin formation by dentin matrix proteins and small extracellular vesicles. *J Endod*. 2021;47(2):253–262. doi:10.1016/j.joen.2020.11.017
63. He X, Dong Z, Cao Y, et al. MSC-derived exosome promotes M2 polarization and enhances cutaneous wound healing. *Stem Cells Int*. 2019;2019:7132708. doi:10.1155/2019/7132708
64. Fu Y, Sui B, Xiang L, et al. Emerging understanding of apoptosis in mediating mesenchymal stem cell therapy. *Cell Death Dis*. 2021;12(6):596. doi:10.1038/s41419-021-03883-6
65. Fuchs Y, Steller H. Live to die another way: modes of programmed cell death and the signals emanating from dying cells. *Nat Rev Mol Cell Biol*. 2015;16(6):329–344. doi:10.1038/nrm3999
66. Doerflinger M, Deng Y, Whitney P, et al. Flexible usage and interconnectivity of diverse cell death pathways protect against intracellular infection. *Immunity*. 2020;53(3):533–547.e537. doi:10.1016/j.immuni.2020.07.004
67. Zhang Y, Chen X, Gueydan C, Han J. Plasma membrane changes during programmed cell deaths. *Cell Res*. 2018;28(1):9–21.
68. Fogarty CE, Bergmann A. Killers creating new life: caspases drive apoptosis-induced proliferation in tissue repair and disease. *Cell Death Differ*. 2017;24(8):1390–1400. doi:10.1038/cdd.2017.47
69. Gupta KH, Goldufsky JW, Wood SJ, et al. Apoptosis and compensatory proliferation signaling are coupled by CrkI-containing microvesicles. *Dev Cell*. 2017;41(6):674–684.e675. doi:10.1016/j.devcel.2017.05.014
70. Lee RH, Pulin AA, Seo MJ, et al. Intravenous hMSCs improve myocardial infarction in mice because cells embolized in lung are activated to secrete the anti-inflammatory protein TSG-6. *Cell Stem Cell*. 2009;5(1):54–63. doi:10.1016/j.stem.2009.05.003
71. Caruso S, Poon IKH. Apoptotic cell-derived extracellular vesicles: more than just debris. *Front Immunol*. 2018;9:1486. doi:10.3389/fimmu.2018.01486
72. Catalano M, O'Driscoll L. Inhibiting extracellular vesicles formation and release: a review of EV inhibitors. *J Extracell Vesicles*. 2020;9(1):1703244. doi:10.1080/20013078.2019.1703244
73. Atkin-Smith GK, Tixeira R, Paone S, et al. A novel mechanism of generating extracellular vesicles during apoptosis via a beads-on-A-string membrane structure. *Nat Commun*. 2015;6:7439. doi:10.1038/ncomms8439
74. Dieudé M, Bell C, Turgeon J, et al. The 20S proteasome core, active within apoptotic exosome-like vesicles, induces autoantibody production and accelerates rejection. *Sci Transl Med*. 2015;7(318):318ra200. doi:10.1126/scitranslmed.aac9816
75. Li M, Xing X, Huang H, et al. BMSC-derived ApoEVs promote craniofacial bone repair via ROS/JNK signaling. *J Dent Res*. 2022;101(6):714–723. doi:10.1177/00220345211068338
76. Liu D, Kou X, Chen C, et al. Circulating apoptotic bodies maintain mesenchymal stem cell homeostasis and ameliorate osteopenia via transferring multiple cellular factors. *Cell Res*. 2018;28(9):918–933. doi:10.1038/s41422-018-0070-2
77. Dou G, Tian R, Liu X, et al. Chimeric apoptotic bodies functionalized with natural membrane and modular delivery system for inflammation modulation. *Sci Adv*. 2020;6(30):eaba2987. doi:10.1126/sciadv.aba2987
78. Lleo A, Zhang W, McDonald WH, et al. Shotgun proteomics: identification of unique protein profiles of apoptotic bodies from biliary epithelial cells. *Hepatology*. 2014;60(4):1314–1323. doi:10.1002/hep.27230
79. Hu H, Dong L, Bu Z, et al. miR-23a-3p-abundant small extracellular vesicles released from Gelma/nanoclay hydrogel for cartilage regeneration. *J Extracell Vesicles*. 2020;9(1):1778883. doi:10.1080/20013078.2020.1778883